
DORY: OVERCOMING BARRIERS TO COMPUTING PERSISTENT HOMOLOGY

A PREPRINT

Manu Aggarwal*

manu.aggarwal@nih.gov
Laboratory of Biological Modeling, NIDDK
National Institutes of Health
31 Center Dr, Bethesda, MD 20892

Vipul Periwal

vipulp@nidk.nih.gov
Laboratory of Biological Modeling, NIDDK
National Institutes of Health
31 Center Dr, Bethesda, MD 20892

March 23, 2021

ABSTRACT

Persistent homology (PH) is an approach to topological data analysis (TDA) that computes multi-scale topologically invariant properties of high-dimensional data that are robust to noise. While PH has revealed useful patterns across various applications, computational requirements have limited applications to small data sets of a few thousand points. We present Dory, an efficient and scalable algorithm that can compute the persistent homology of large data sets. Dory uses significantly less memory than published algorithms and also provides significant reductions in the computation time compared to most algorithms. It scales to process data sets with millions of points. As an application, we compute the PH of the human genome at high resolution as revealed by a genome-wide Hi-C data set. Results show that the topology of the human genome changes significantly upon treatment with auxin, a molecule that degrades cohesin, corroborating the hypothesis that cohesin plays a crucial role in loop formation in DNA.

Keywords T

topological data analysis, multi scale, algorithm, large data sets, genome structure

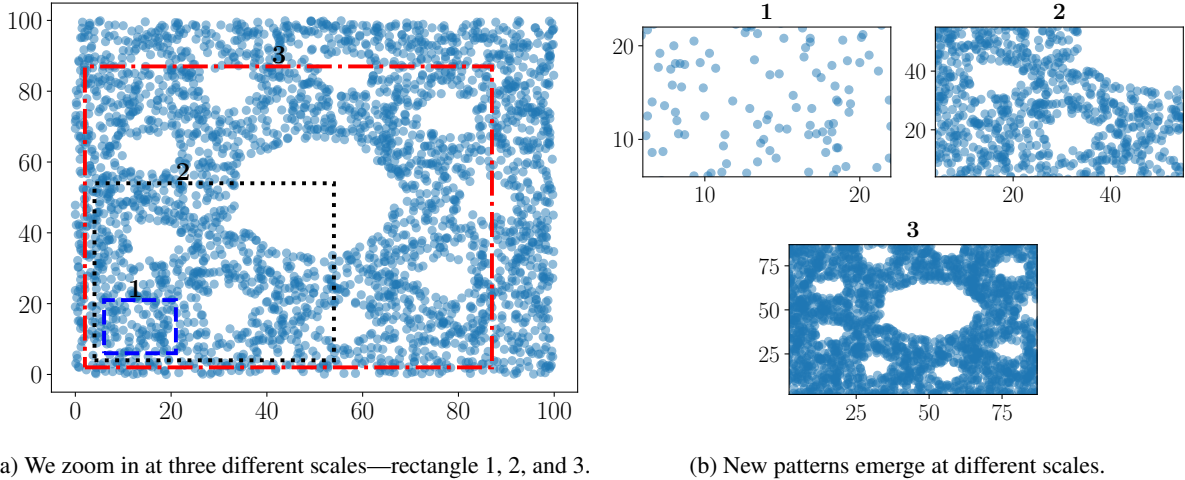
1 Introduction

The ever increasing availability of scientific data necessitates development of mathematical algorithms and computational tools that yield testable predictions or give mechanistic insights into model systems underlying the data. The utility of these algorithms is determined by the validity of their theoretical foundations, the generality of their applications, their ability to deal with noisy, high-dimensional, and incomplete data, and the computational scalability. Persistent homology (PH), a mathematically rigorous approach to topological data analysis (TDA), finds patterns in high-dimensional data that are robust to noise, providing a multi-scale overview of the topology of the data.

For example, consider a point-cloud data set of 3000 points (Figure 1a). The three rectangles (Figure 1b) show different scales of observation of the data. At the small spatial scale (rectangle 1), we do not see a discernible pattern, at a larger scale (rectangle 2), two holes with a distinct pattern appear, and increasing the scale further reveals a third distinct pattern, the large hole at the center (rectangle 3). For this data set, PH will compute that there are three groups of

*Corresponding author

topologically distinct features. It will also indicate the scale at which they emerge. However, this analysis comes at a high computational cost that has limited the applicability of PH to very small data sets. To introduce these extant computational limitations, we briefly introduce some terminology. A general and detailed exposition on persistent homology can be found in Edelsbrunner and Harer [2008].



(a) We zoom in at three different scales—rectangle 1, 2, and 3.

(b) New patterns emerge at different scales.

Figure 1: A simulated data set with 3000 points.

To formalize the notion of topology of a discrete data set, a collection of so-called simplices is defined from the data set as follows: An n -simplex is a set of $n + 1$ points and is said to have dimension n ($\dim-n$). Figure 2a shows different ways to interpret a simplex—as a mathematical set, graphical object, or geometric object—in different dimensions. The *boundary* of an n -simplex σ , denoted $\partial\sigma$, is the set of all $(n - 1)$ -simplices contained in the simplex. The *coboundary* of an n -simplex σ , denoted $\delta\sigma$, is the set of all $(n + 1)$ -simplices ω such that $\sigma \in \partial\omega$. A collection of simplices is called a *complex*. Figure 2b shows examples of coboundaries and complexes. Contraction can be visualized as a continuous deformation of a simplex to a point. Non-contractible topological structures correspond to obstructions to such a contraction, suggesting the possible existence of a feature in the data.

A hole in $\dim-d$ is a complex that has a non-contractible boundary in $\dim-(d - 1)$. The complex D' in Figure 2b contains the simplex $\{a, b, c\}$, and hence its boundary $\partial\{a, b, c\} = \{\{a, b\}, \{b, c\}, \{c, a\}\}$ will contract in $\dim-1$. On the other hand, since the complex D does not contain $\{a, b, c\}$, its boundary $\partial\{a, b, c\}$ cannot contract in $\dim-1$. Hence, D contains a non-contractible structure or a hole. These non-contractible structures in $\dim-d$ define the *homology group* for $\dim-d$, denoted by H_d , partitioned into equivalence classes that are related by contractible simplices. For example, the homology group H_1 of the complex D has one equivalence class. The non-contractible structures in H_0 can be mapped to path-connected components when the complex is viewed as a discrete graph. Those in H_1 can be mapped to holes on the surface of the triangulation of the point cloud, but are more commonly referred as *loops*, indicative of one dimensional boundaries around the holes. In H_2 they can be thought of as *voids* in an embedding of the triangulation in a three-dimensional metric space, and sets of triangular faces will define their boundaries.

To give a multi-scale overview, PH tracks changes in the homology groups as the scale of observation changes. We see that the collection of simplices in the data set, otherwise known as the complex of the data set, changes at different spatial scales as its construction is based on pairwise distances in the discrete data set. The example (Figure 3) shows 4 points in a metric space, with the numbers between two points representing the spatial pairwise distances ($d(x, y)$). At any given scale of observation τ we build a complex with all of the 1-simplices $\{a, b\}$ such that $d(x, y) \leq \tau$. Additionally, to compute H_d , all $(d + 1)$ -simplices whose boundary is in the complex are also added to it. *This results in a factorial increase in the number of simplices to consider in the complex scaling as the number of points in the data set is raised to a power two larger than the dimension of the homology group.* In Figure 3, when $\tau = 0$, there are 4 points or 0-simplices. These are indexed arbitrarily from σ_0 to σ_3 . Starting from $D_0 = \{\sigma_0\}$, we define a sequence of complexes $D_0 \subset D_1 \subset \dots \subset D_n$ such that $D_i = D_{i-1} \cup \{\sigma_i\}$. At $\tau = 0$, we have $D_3 = \{\sigma_0, \sigma_1, \sigma_2, \sigma_3\}$. As τ increases, more simplices are added to the complex, and the sequence (D_0, \dots, D_{11}) can be computed for this example. Simplices that are added to the complex at the same value of τ can be ordered arbitrarily relative to each other. This sequence of complexes is called the *Vietoris-Rips filtration*.

For every complex in the VR-filtration, we compute the homology groups and record changes in them as we process complexes in the filtration. For example, there is the birth of a hole (equivalently, a loop) in H_1 when σ_8 is added, which

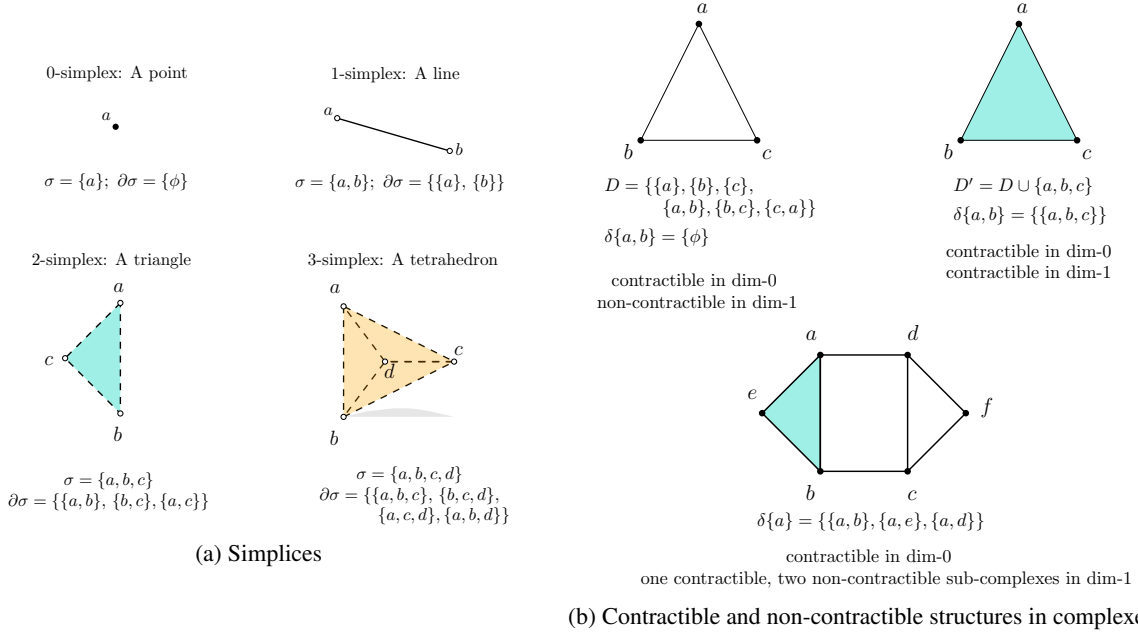


Figure 2: Simplicies form the building blocks for defining a topological space on discrete data set, simplicial topology.

contracts or dies when σ_{11} is added. Birth-death pairs are called persistence pairs, and they are plotted as a function of the scale, τ . In our example, the persistence pair is (σ_8, σ_{11}) in H_1 . These pairs gives us *persistence diagrams* (PD), one for every H_d that is computed. The persistence diagram corresponding to H_1 for this example will contain exactly $(2.5, 2.75)$, since σ_8 is added at $\tau = 2.5$ and σ_{11} is added at $\tau = 2.75$. The persistence diagram for the example in Figure 1a is shown in Figure 4b.

It has been shown that the same persistence diagram can be obtained by computing cohomology groups, denoted by H_d^* . If (σ, τ) is a persistence pair in H_d , then (τ, σ) is a persistence pair in H_d^* , and consequently, $|H_d| = |H_d^*|$. Moreover, the algorithms that compute the persistence pairs of H_d can also be used to compute the persistence pairs of H_d^* by applying them to the coboundaries of the complexes in the filtration [De Silva et al., 2011].

As discussed above, computing H_2 across all scales of a data set requires storing and processing all 3-simplices, that is, $O(n^4)$ simplices. Even for a small data set with $n = 500$ data points, the number of 3-simplices is $\binom{500}{4} = 2573031125$, indicative of the memory required to represent the filtration in the computer. Different methods have been developed for storing this information. We compare our algorithm with three software packages—Gudhi, Ripser, and Eirene. Gudhi represents the filtration using a simplex tree [Boissonnat and Maria, 2014], and Ripser [Bauer, 2019] represents a simplex using combinatorial indexing. For large data sets, creating a simplex tree for the entire filtration a priori can require memory up to $O(n^4)$, and indexing simplices using combinatorial indexing overflows the bounds of integer data types in most computer architectures. Therefore, both these methods cannot process data sets with large numbers of points. Eirene uses matroid theory that takes more memory than Ripser and, in some cases, more memory than Gudhi. All packages failed to compute PH for at least one data set in our experiments. None were able to process the data set of interest to us, the conformations of the human genome, because of such practical limitations. As PH computation requires processing a combinatorially large number of simplices as well, any method for reducing memory requirements had better not be accompanied by an inordinate increase in computation time either.

Due to these computational difficulties, published algorithms have been practically limited to computing topological features up to and including H_2 . This still allows for applications of PH to a large class of data sets in the physical sciences or to low-dimensional embeddings of high-dimensional data. Therefore, we focus on computing topological features only up to and including the first three dimensions. We take advantage of this restriction to devise a new way to store information and new algorithms to process it, resulting in a reduction in memory requirements by orders of magnitude accompanied with reduced computation time in almost all our test cases.

The two meter long human DNA fits into a nucleus with an average diameter of $10 \mu\text{m}$ by folding into a complex, facilitated by many proteins which play functional and structural roles [Rowley and Corces, 2018]. This folding is believed to have functional significance so determining topological features like loops and voids in the folded DNA

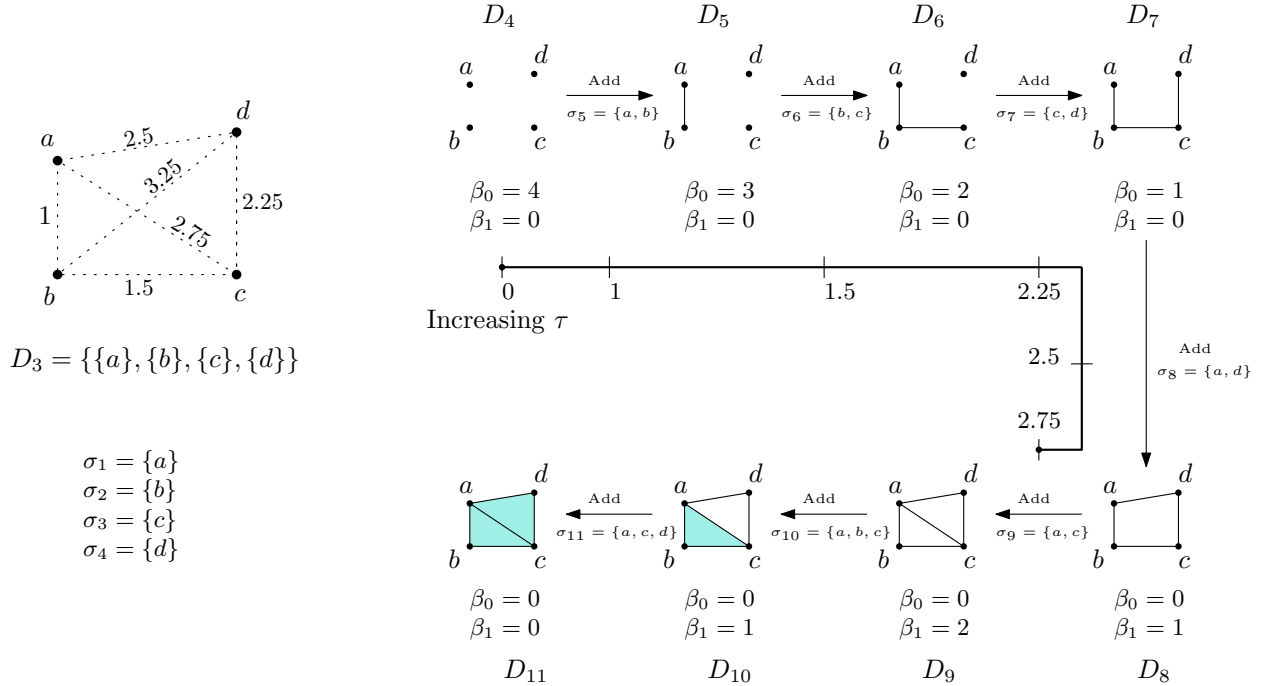


Figure 3: Topological features—number of components (β_0) and holes (β_1)—change as the scale of observation (τ) changes.

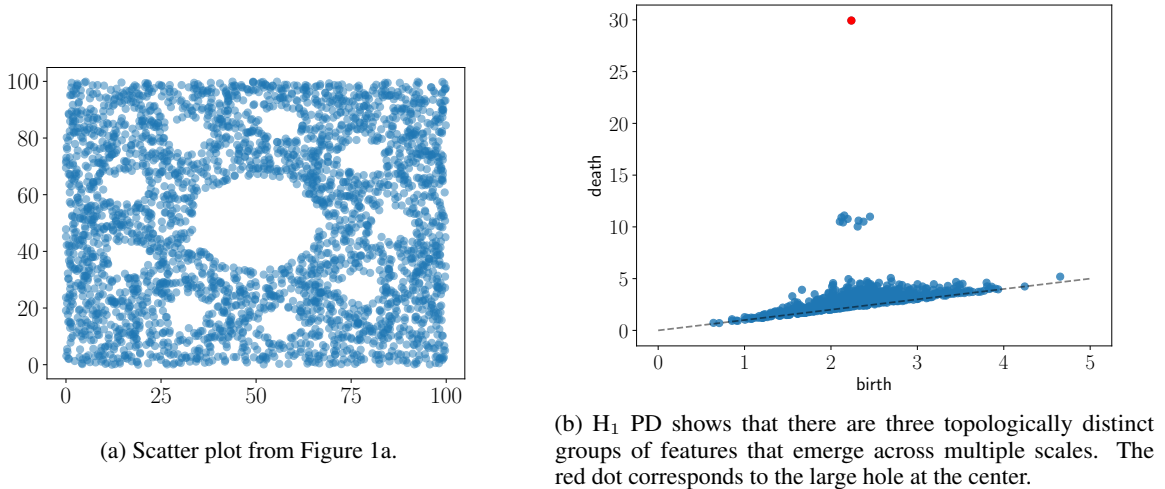


Figure 4: Scatter plot of the data set and its H_1 persistence diagram.

is of interest. Hi-C experiments estimate pairwise spatial distances between genomic loci at 1 kilobase resolution genome [Lieberman-Aiden et al., 2009]. The resulting data set of around 3 million points is analyzed by our algorithm in approximately ten minutes.

Cohesin is a ring-shaped protein complex that has been shown to colocalize on chromatin along with a highly expressed protein, CTCF, at anchors of loops in the folded chromosome [Rao et al., 2014], indicative of its importance for loop formation in DNA. The H_1 PD corroborates the result of Rao et al. [2017]—cohesin is crucial for loop formation in DNA because, upon addition of auxin, an agent that is known to impair cohesin, the elimination of loops is observed. Additionally, the H_2 PD reveals that auxin treatment leads to a significant reduction in the number of voids.

The rest of this paper is structured as follows: Section 2 introduces the algorithms that form the foundations of Dory. We summarize our contributions in Section 3. The algorithm for Dory is explained in Section 4. It is then tested with

pre-established data sets, and computation time and memory taken are compared with published algorithms in Section 5. The analysis of human genome conformations using Hi-C data is in Section 6. We end with a discussion in Section 7.

2 Algorithmic Background

An algorithm to compute the persistence birth-death pairs was given by Edelsbrunner et al. [2000], then reformulated as a matrix reduction in Cohen-Steiner et al. [2006]. Any given filtration, viewed as a set of sequences of simplices $(\sigma_i)_{1 \leq i \leq N}$, can be represented as a *boundary matrix* $D = (d_{ij}) \in \mathbb{R}^{N \times N}$, where $d_{ij} = 1$ if σ_i is a boundary element of σ_j , and is otherwise 0. Consequently, the indices of the columns and rows of D represent the simplices indexed according to their order in the filtration. We begin by defining a matrix $R = D$. Then, $\text{low}(j)$ is defined as the largest row index of the non-zero element in column j of R , that is, $\text{low}(j) = \text{argmax}\{d_{ij} = 1\}$. The matrix reduction of R is formalized as adding (modulo 2) column j with column i , for $i < j$, until $\text{low}(j)$ is a *pivot* entry—the first non-zero entry in the row with index $\text{low}(j)$ is at column j . This can be written as a matrix multiplication $DV = R$ (see Figure 5a), where V is the matrix that stores reduction operations and R is the resulting matrix with all of its columns reduced. In this work we specifically consider addition (modulo 2) of columns for applications to spatial point-cloud data sets. This reduction can be carried out in two ways—standard column algorithm (appendix A, algorithm 4) and standard row algorithm (appendix A, algorithm 5). When all columns of R have been reduced, the persistence pairs are given by $(\sigma_{\text{low}(j)}, \sigma_j)$ (born when $\sigma_{\text{low}(j)}$ is added and died when σ_j is added). Further, if column j was reduced to $\mathbf{0}$ but j is not a pivot of any column of R , then there is a non-contractible structure in the final complex that was born when σ_j was added to the filtration but it never contracted or died. We represent such a pair by (σ_j, ∞) .

The same V and, consequently, the same R are obtained for the standard column and row algorithms [De Silva et al., 2011]. Moreover, reduction of the coboundaries yields the persistence pairs for the cohomology groups, H_d^* , that are in one-to-one correspondence with the persistence pairs of H_d . The coboundary matrix is denoted by $D^\perp = (d_{ij}) \in \mathbb{R}^{N \times N}$, where $d_{ij} = 1$ if σ_{N-i+1} is in the coboundary of σ_{N-j+1} , and is otherwise 0. In other words, the columns of D^\perp are coboundaries, and the indices of the columns and rows of D^\perp are simplices ordered in the reverse order of the filtration sequence. The matrix setup is shown in Figure 5b. De Silva et al. [2011] observed empirically that computing cohomology via the row algorithm provides improvements over homology computation in both time taken and memory requirement.

Figure 5 indicates the size of the matrices when computing PH up to and including the first three dimensions for VR-filtration of a data set with n points. If $\tau = \infty$, the filtration will admit $\binom{n}{0} + \binom{n}{1} + \binom{n}{2} + \binom{n}{3} + \binom{n}{4} \approx O(n^4)$ simplices (all of the possible 0-, 1-, 2-, and 3-simplices). For a data set with as few as 500 points, the memory requirement just to store D in a sparse format (storing only the indices of the non-zero elements) is more than 41 GB (presuming 4 bytes per unsigned int).

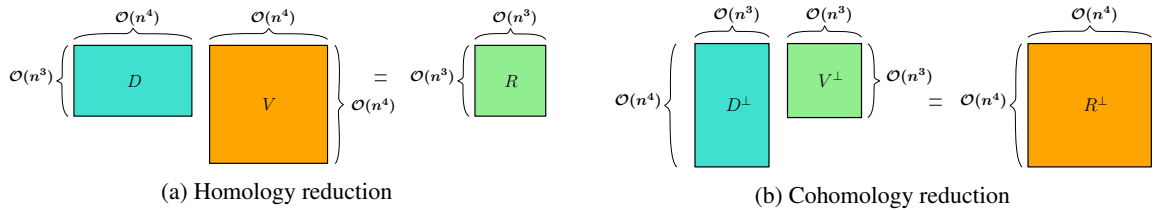


Figure 5: Matrix representation and bounds of PH computation for a data set with n points.

3 Our Contribution

- A new way to index 2- and 3-simplices that significantly reduces memory requirement and also aids in reducing computation time.
- Algorithms to compute coboundaries for edges and triangles using our indexing method that optimize computation time of coboundary traversal during reduction.
- A fast implicit column algorithm to compute PH that can potentially reduce memory usage by a factor of the number of points in the data set without an inordinate increase in the computation time.
- Serial-parallel algorithm that distributes computation of PH over multiple threads without a significant increase in the total memory requirement.

- A computation of the PH of the human genome at high resolution, a data set with millions of points.
- Two versions of code—sparse and non-sparse. The sparse version requires memory proportional to the number of permissible edges in the filtration. The non-sparse version, while faster, requires memory proportional to the number of total edges possible in the data set.

4 Our Algorithm

The aim is to compute persistence pairs up to three dimensions for VR-filtration. We will refer to the 0-simplices as vertices (v), 1-simplices as edges (e), 2-simplices as triangles (t), and 3-simplices as tetrahedrons (h). Consider a point-cloud data set embedded in a metric space, that is, there is a well-defined distance metric between any two points (vertices) in the space. We denote the number of vertices by n . The number of edges in the filtration, denoted by n_e , will depend upon the maximum permissible value of the filtration parameter, denoted by τ_m . If τ_m is small compared to the maximum distance in the data set, we expect $n_e \ll \binom{n}{2}$ and we call the filtration *sparse*. Since the reduction operations are always between complexes of the same dimension, we construct VR-filtrations for each dimension separately. Let \mathcal{S}^d be the set of all permissible simplices of dimension d and \mathcal{O}^d be the corresponding set of orders in the filtration. We define bijective maps $f_d : \mathcal{S}^d \rightarrow \mathcal{O}^d$. Since all vertices are born at the same filtration parameter (zero), $f_0(v)$ for a vertex v can be arbitrarily assigned a unique whole number. For convenience, we will use $f_0(v)$ and v interchangeably. For edges, the map $f_1(e)$ is the indexing defined by the sorting algorithm applied to the lengths of the edges. The filtration for 0-simplices is then the list of vertices ordered according to f_0 , and is denoted by F_0 . The filtration for 1-simplices is a list of edges ordered according to f_1 , and is denoted by F_1 . Additionally, we will denote the list of d -simplices in the reverse order of filtration by F_d^{-1} . To define filtrations for 2- and 3-simplices we introduce a new way to index triangles and tetrahedrons.

4.1 Paired-indexing and Neighborhoods

We first define the *diameter* of a simplex σ in the filtration as the maximum of the orders of the edges in the simplex, denoted by $d(\sigma)$. The corresponding edge is denoted by $d^{-1}(\sigma)$. Then, *paired-indexing* uses a pair of keys, primary (k^p) and secondary (k^s), denoted by $\langle k^p, k^s \rangle$. The primary key for both triangles and tetrahedrons is their diameter and the secondary key is the order of the simplex defined by the remaining points. For a triangle $t = \{a, b, c\}$, if $d^{-1}(t) = \{a, b\}$, then $f_2(\{a, b, c\}) = \langle f_1(\{a, b\}), f_0(\{c\}) \rangle = \langle f_1(\{a, b\}), c \rangle$. For a tetrahedron $h = \{a, b, c, d\}$, if $d^{-1}(h) = \{a, b\}$, then, $f_3(\{a, b, c, d\}) = \langle f_1(\{a, b\}), f_1(\{c, d\}) \rangle$. We define an ordering on the paired-indexing as follows,

$$\langle k_i^p, k_i^s \rangle > \langle k_j^p, k_j^s \rangle \text{ iff either } \{k_i^p > k_j^p\} \text{ or } \{k_i^p = k_j^p \text{ and } k_i^s > k_j^s\}. \quad (1)$$

This ordering on the paired-indexing preserves the order of the simplices in the VR-filtration since a simplex with the larger diameter will have a greater order in the filtration. Simplices with the same diameter can be ordered arbitrarily with respect to each other, which in paired-indexing is based on the secondary key. The maps f_2 and f_3 then define filtrations F_2 and F_3 , respectively. We do not store these filtrations as lists in the algorithm and instead compute them on the fly, reducing the memory required. We say that a simplex in \mathcal{S}^d is greater than another simplex in \mathcal{S}^d iff its order in the filtration is greater.

The paired-indexing plays an important role in both reducing memory requirements and computation time. Using the 4 byte unsigned int, this indexing will take exactly 8 bytes to represent any triangle or tetrahedron in a filtration regardless of the number of points in the data set. Further, since k^p and k^s are less than n_e , the paired-indices are bounded by $\mathcal{O}(n_e)$, rather than $\mathcal{O}(n^4)$. This specifically reduces memory requirement by many orders of magnitude for sparse filtrations, where $n_e \ll \binom{n}{2}$.

4.2 Computing Coboundaries

We show how paired-indexing can be used to compute coboundary of edges and triangles. We begin by defining *vertex-neighborhood* (N^a) and *edge-neighborhood* (E^a) of a vertex a . The neighbor of the vertex a is a vertex that shares an edge with a . Both N^a and E^a are lists of all neighbors of a . Each element of these lists is a structure that contains a neighbor of a and the order of the edge between them. The vertex-neighborhood is sorted by the order of the neighbors and the edge-neighborhood is sorted by the order of the corresponding edges (see Figure 6). The vertex and edge neighborhoods of all vertices are computed using F_0 and F_1 , and they are stored in the memory. We will use F_0 and F_1 in Figure 6 as an example to illustrate how paired-indexing can be used to compute coboundary of an edge and a triangle. For convenience, the order of an edge $\{a, b\}$, $f_1(\{a, b\})$, is denoted by ab .

F_0	a	b	c	d	e	f	g	h						
F_1	de	ah	bh	ae	be	eh	ac	bf	ab	ad	bg	af	bd	ef

N^a	neighbor	b	c	d	e	f	h
	$f_1(\text{edge})$	ab	ac	ad	ae	af	ah

E^a	neighbor	h	e	c	b	d	f
	$f_1(\text{edge})$	ah	ae	ac	ab	ad	af

Figure 6: An example of a VR-filtration. F_0 is the list of vertices and F_1 is the list of edges, both sorted in the order of the filtration. The vertex- and edge-neighborhoods for vertex a are shown as example. The dark border indicates that N^a is sorted by the order of neighbors of a and E^a is sorted by the order of the corresponding edges.

4.2.1 Coboundaries of Edges

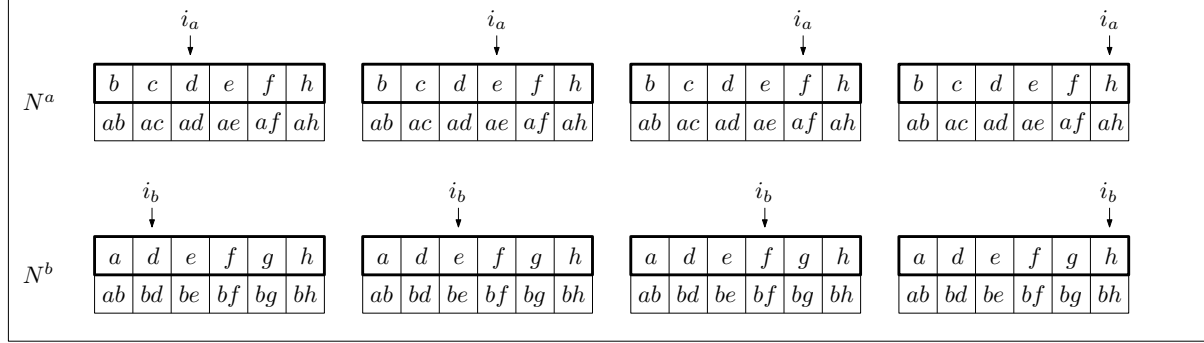
Consider the edge $\{a, b\}$ in Figure 6. Any simplex in its coboundary is a triangle $t = \{a, b, v\} = \langle k_1, k_2 \rangle$, where v is a common neighbor of a and b , and the diameter of $t = k_1 \geq ab$. We consider two cases: case 1, triangles with diameter equal to ab , and case 2, triangles with diameter greater than ab . The triangles in case 1 are smaller than those in case 2. Hence, to compute the simplices in the coboundary as ordered in F_2 , we start in case 1—the primary key is ab and the order of the simplices is decided by the vertex in t that is not a and b , that is, v . We traverse along the vertex-neighborhoods using indices i_a and i_b to find common neighbors in an increasing order. Initially, both are set to 0. As shown in Figure 7, we increment the index pointing to the lower ordered vertex till both indices point to the same vertex v , in which case, v is a common neighbor and $\{a, b, v\}$ exists in the filtration. However, we have to ensure that its diameter is ab since we are in case 1. For example, in (1) in Figure 7, we skip $\{a, b, d\}$ because $ad > ab$ (see F_1 in Figure 6). Note that the structures in vertex-neighborhoods give direct access to av and bv at i_a and i_b for comparison with ab . Otherwise, if the diameter of $\{a, b, v\} = ab$, then $\langle ab, v \rangle$ is the next greater triangle in $\delta\{a, b\}$ in F_2 . This triangle is recorded as $\phi = (ab, i_a, i_b, \delta_*)$ where $\delta_* = f_2(\{a, b, v\}) = \langle ab, v \rangle$. We call this the ϕ -representation of δ_* as a simplex in the coboundary of $\{a, b\}$. If either of the indices reach the end of the corresponding neighborhood, we go to case 2.

In case 2, the triangles in $\delta\{a, b\}$ have diameter greater than ab . Hence, their order in the filtration is defined by the diameter of the primary key. To compute the primary keys as ordered in F_2 , we define i_a and i_b to be indices of the respective edge-neighborhoods since they are sorted by the order of the edges. We set i_a and i_b to point to the smallest edges greater than ab (binary search operations in E^a and E^b , respectively). We then consider the index that points to the lower ordered edge. For example, in (7) in Figure 7, $i_a = 3$ points to ad and $i_b = 3$ points to bg . We consider $i_a = 3$ because $ad < bg$. Now, we have to check that $\{a, b, d\}$ exists and its diameter is ad . A single binary search operation over N^b finds that d is a neighbor of b , confirming the existence of $\{a, b, d\}$, and it also gives us bd . Since $ad < bd$, the diameter of $\{a, b, d\}$ is not ad and we do not record it as a coboundary. We proceed by incrementing i_a by one. Now i_b points to the smaller edge, and the corresponding triangle is $\{a, b, g\}$. A binary search over N^b finds that g is not a neighbor of a , hence, this triangle does not exist, and i_b is incremented by 1 to continue. The index i_a now points to the smaller edge (af), and the corresponding triangle is $\{a, b, f\}$. Since, this triangle exists and af is its diameter, $\langle af, b \rangle$ is the next simplex in the coboundary and it is recorded as $\phi = (ab, i_a, i_b, \langle af, b \rangle)$. This process is continued till both i_a and i_b reach the end of the respective edge-neighborhood.

The above computation yields the coboundary of $\{a, b\}$ as a list of tuples ϕ_{ab}^i (see Figure 7) in an increasing order. This is an inefficient method to compute the coboundary of a simplex if it needs to be computed only once. A faster method would be to create the entire list of simplices in the coboundary and sort it by the order. However, reduction can require the computation of the coboundary of a simplex multiple times. Further, it is not feasible to store the entire coboundary matrix a priori due to memory limitations—even the size of the coboundary of one simplex can be up to $O(n^4)$ (see Figure 5). Using our ϕ -representation, we implement three algorithms to address both these issues. First, the smallest simplex in the coboundary of $\{a, b\}$ can be found simply by starting in case 1 with i_a and i_b initialized to 0, and we proceed as outlined previously. The first valid simplex encountered is the answer. This is implemented as `FindSmallestt` (algorithm 8). Second, given a tuple $\phi = (ab, i_a, i_b, \langle k_1, k_2 \rangle)$, the next greater simplex in $\delta\{a, b\}$ can be computed as follows. If $k_1 = ab$, then i_a and i_b are indices of the vertex-neighborhoods (case 1) and if $k_1 > ab$, they are indices of edge-neighborhoods (case 2). After determining the scenario, we proceed as outlined previously. As a result, given the ϕ -representation of a triangle t in the coboundary of an edge $\{a, b\}$, we can compute the next greater triangle in its coboundary without always having to traverse entire neighborhoods of a and b . We implement this as `FindNextt` (algorithm 9). Third, given a triangle $\delta_{\#} = \langle k_1, k_2 \rangle$, the smallest simplex greater than or equal to $\delta_{\#}$ in

the coboundary of an edge $\{a, b\}$ can be computed by considering three scenarios. (1) If $k_1 < ab$, then the triangle with the least order in the coboundary of $\{a, b\}$ is the answer. (2) If $k_1 = ab$, then we start in case 1 at indices i_a and i_b of vertex-neighborhoods that point to the neighbor with smallest order greater than or equal to k_2 . If no such neighbor exists, then we initialize i_a and i_b to the beginning of case 2. (3) If $k_1 > ab$, then we start in case 2 at the indices i_a and i_b of edge-neighborhoods that point to the edges with smallest order greater than or equal to k_1 . This is implemented as FindGEQt (algorithm 10). Note that the search operations in all of these algorithms are binary search operations since vertex- and edge-neighborhoods are sorted. We will show in 4.3.2 how these three algorithms are utilized to reduce the coboundaries to compute persistence pairs. See appendix B for all pseudocode related to coboundaries of edges.

Case 1



(1)

(2)

(3)

(4)

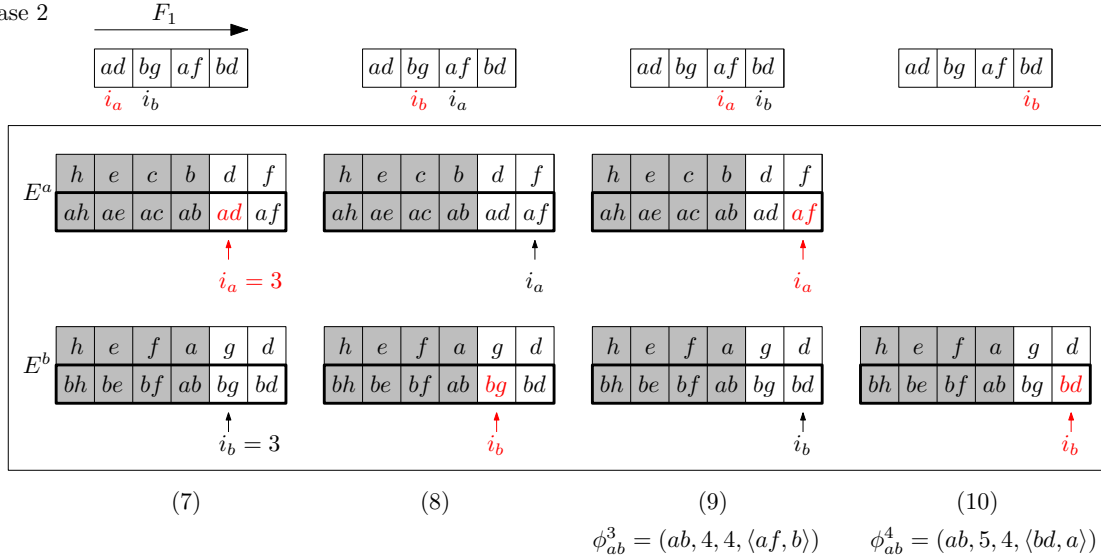
$$\phi_{ab}^0 = (ab, 3, 2, \langle ab, e \rangle)$$

$$\phi_{ab}^1 = (ab, 4, 3, \langle ab, f \rangle)$$

$$\phi_{ab}^2 = (ab, 5, 5, \langle ab, h \rangle)$$

i_a reached end
go to Case 2

Case 2



(7)

(8)

(9)

(10)

$$\phi_{ab}^3 = (ab, 4, 4, \langle af, b \rangle)$$

$$\phi_{ab}^4 = (ab, 5, 4, \langle bd, a \rangle)$$

Figure 7: Using vertex- and edge-neighborhoods to compute simplices in the coboundary of edge $\{a, b\}$ (see Figure 6 for F_1), such that they are in the order of F_2 . The valid triangles are stored using ϕ -representation.

4.2.2 Coboundaries of Triangles

Consider the triangle $t = \{a, b, e\} = \langle ab, e \rangle$ in Figure 6. Any simplex in its coboundary is a tetrahedron $t = \{a, b, e, v\} = \langle k_1, k_2 \rangle$, where v is a common neighbor of a, b , and e , and the diameter of $h = k_1 \geq ab$. We will use three indices, i_a, i_b , and i_e , to keep track of neighborhoods of a, b , and e , respectively. We consider two cases: case 1, tetrahedrons with diameter equal to ab , and case 2, tetrahedrons with diameter greater than ab . The tetrahedrons in case 1 are smaller than the triangles in case 2, so we start with case 1—the primary key is ab and the order of the simplices is decided by the order of the edge $\{e, v\}$. To compute such edges according to their order in F_1 , we traverse through the

edge-neighborhood of e . Initially, i_e is set to 0. For every edge $\{e, v\}$ that i_e points to, we check whether v is a neighbor of a and b to confirm existence of $\{a, b, e, v\}$, and we check that ab is its diameter. These checks require two binary search operations, one each for N_a and N_b . If both conditions are satisfied, then we record the tetrahedron. We proceed by incrementing i_e by one. For example, when $i_e = 0$ in (1) in Figure 8, the resulting tetrahedron exists but ab is not its diameter, and we do not record it. We skip when i_e points to ae or be because they are not valid tetrahedrons. The first tetrahedron with diameter ab is when $i_e = 3$, and hence, $\{a, b, e, h\}$ is the smallest tetrahedron in δt . We define the ϕ -representation for tetrahedrons as the tuple $\phi = (t, i_a, i_b, i_e, f, \langle ab, eh \rangle)$, where f flags the diameter as follows— f is 0, 1, 2, 3, and 4 correspond to diameter being $ab, ah, bh,$ and eh , respectively. This flag is implemented to determine which index has to be incremented to find the next greater tetrahedron in δt . For example, if ab is the diameter, that is, $f = 0$, we are in case 1 and i_e is to be incremented by one to proceed. Note that, in general, for any given triangle $t = \langle k^p, k^s \rangle$, we compute $a \leftarrow \min\{f_1^{-1}(k^p)\}$, $b \leftarrow \max\{f_1^{-1}(k^p)\}$, and $e \leftarrow k^s$. Case 1 is continued till i_e points to an edge greater than ab , since all tetrahedrons henceforth will have a diameter greater than ab . In Figure 6, $ef > ab$ (indicated by a dashed line), hence we start with case 2 when $i_e = 3$.

All valid tetrahedrons in case 2 that are in δt will have diameter greater than ab . The index i_e already points to the entry in E^e that has the smallest edge greater than ab . We implement binary search to compute i_a and i_b such that they also point to the smallest edge greater than ab in the respective edge-neighborhood. All tetrahedrons in case 2 will have different primary keys since they have different diameters. Among the indices $i_a, i_b,$ and i_e , we consider the index that is pointing to the edge with the minimum order. As before, we have to check the existence of the tetrahedron and that its diameter is the edge under consideration. For example, in Figure 8, we begin case 2 in (5) by considering i_a because it points to $ad = \min\{ad, bg, ef\}$. Binary searches for vertex d over N^b and N^e confirm the existence of the tetrahedron $\{a, b, e, d\}$ and also show that ad is not its diameter. Hence, this tetrahedron is not recorded and i_a is incremented by 1 to proceed. Now, i_b points to the smallest edge, but the resulting tetrahedron does not exist since g is not a neighbor of e . The smallest tetrahedron in case 2 is $\{a, b, e, d\}$, recorded at (8) as $(\langle ab, e \rangle, 6, 5, 4, 2, \langle bd, ac \rangle)$. Note that f is 2 since the diameter is bd . This flag dictates that i_b is to be incremented by 1 to proceed because the current pointer being considered is i_b . Similarly, if $f = 1$ then ad is the diameter and i_a has to be incremented to proceed and if $f = 3$, then ed is the diameter and i_e has to be incremented by 1. The index i_e is incremented to proceed when either $f = 0$ or $f = 3$, but we are in case 1 in the former and in case 2 in the latter. Case 2 ends when all three indices reach the end of their respective edge-neighborhood.

The above computation yields the coboundary of $t = \{a, b, e\}$ as a list of tuples ϕ_t^i (see Figure 8). The case and the index to be incremented is determined by the flag f as discussed previously. As done for edges, this ϕ -representation is used to implement three algorithms—FindSmallesth, FindNexth, and FindGEQh. The smallest simplex in the coboundary of t can be found simply by starting in case 1, initializing i_e to 0, and proceeding as outlined previously. The first valid simplex encountered is the answer (algorithm 13). For FindNexth (algorithm 14), given the ϕ -representation of a simplex $\langle k_1, k_2 \rangle$ in δt as $\phi = (t, i_a, i_b, i_e, f, \langle k_1, k_2 \rangle)$, the smallest simplex greater than $\langle k_1, k_2 \rangle$ in δt can be computed by proceeding in case 1 if $f = 0$ and proceeding in case 2 otherwise—incrementing the indices by one as dictated by the value of f . Finally, given a tetrahedron $\delta_{\#} = \langle k_1, k_2 \rangle$, the search for the smallest simplex greater than or equal to $\delta_{\#}$ in δt is optimized by considering three scenarios (algorithm 15). (1) If $k_1 < ab$, then the smallest tetrahedron in δt (FindSmallesth) is the answer. (2) If $k_1 = ab$, then we start in case 1 and search for i_e that points to the smallest edge greater than or equal to k_2 . If no such edge exists, then we start in case 2 with i_e pointing to the end of E^e . (3) If $k_1 > ab$, we are in case 2 and we find the indices that are greater than or equal to k_1 in the respective edge-neighborhoods. See appendix C for all the pseudocode related to coboundaries of triangles.

4.3 Cohomology Reduction

To compute persistence pairs using cohomology reduction, we reduce one simplex at a time since it is often not feasible to store the coboundary matrix D^{\perp} . Suppose the reduced coboundaries are stored in R^{\perp} and the reduction operations are stored in V^{\perp} . We will denote the column in R^{\perp} that contains the reduced coboundary of edge e by $R^{\perp}(e)$ and the corresponding column in V^{\perp} by $V^{\perp}(e)$. Using this notation, the column reduction to reduce coboundary of one edge at a time is shown in algorithm 1. Here, $\text{low}(R^{\perp}(e))$ is the simplex with the smallest order in column $R^{\perp}(e)$. The partial reduction of the edge is stored in r which initially is the coboundary of the edge. If $\text{low}(r) = \text{low}(R^{\perp}(e'))$ for some edge e' , then r is reduced (sum modulo 2) with $R^{\perp}(e')$. If no such edge exists or if r is $\mathbf{0}$, then r is completely reduced. A non-empty completely reduced r is recorded as the column $R^{\perp}(e)$ or R^{\perp} , and $(\text{low}(R^{\perp}(e)), e)$ is a persistence pair.

4.3.1 Improving Scalability of Memory Requirement

However, Figure 5b shows that R^{\perp} has the worst bounds on size. Therefore, we store only the reduction operations, that is, V^{\perp} . Then, r can be implicitly reduced with $R^{\perp}(e')$ by summing (modulo 2) it with the coboundaries of edges in $V^{\perp}(e')$ (see algorithm 2). This algorithm is implemented in Ripser. The smallest simplex t after reducing coboundary

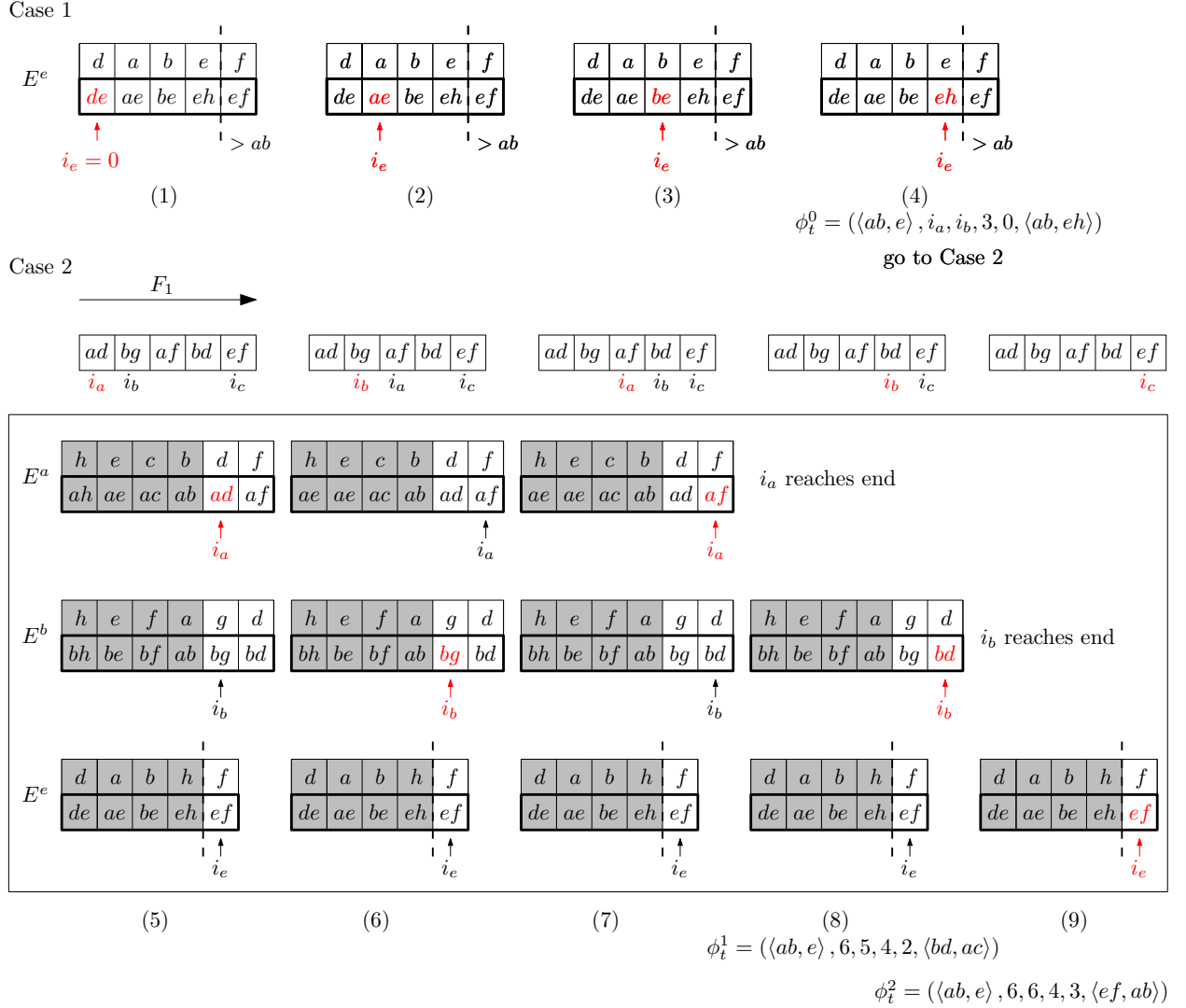


Figure 8: Using edge-neighborhoods to compute simplices in the coboundary of triangle $\{a, b, e\}$ (see Figure 6 for F_1), such that they are in the order of F_3 . The index marked in red in every iteration, points to the edge under consideration. The valid tetrahedrons are stored using ϕ -representation.

Algorithm 1 Starting with standard column reduction

- 1: **Input:** F_1
 - 2: R^\perp is empty
 - 3: **for** e in order of F_1^{-1} **do**
 - 4: $r \leftarrow \delta e$
 - 5: **while** r not empty AND there exists edge e' s.t. $\text{low}(R^\perp(e')) = \text{low}(r)$ **do**
 - 6: $r \leftarrow r \oplus R^\perp(e')$
 - 7: **if** r not empty **then**
 - 8: $R^\perp(e) \leftarrow r$
-

of an edge e' is stored as a persistence pair (t, e') in p^\perp . In this algorithm, the partial reduction operations are recorded in v , the result of the ongoing reduction is in r , and the smallest simplex in r is stored as δ_* . However, keeping track of r can require a lot of computer memory as its length is bounded by $O(n^3)$ (and by $O(n^4)$ when reducing triangles). We begin by proposing an implicit row algorithm that does not store r at any stage of reduction, and it implicitly reduces r using v . Hence, its memory requirement depends on the size of v — $O(n^2)$ for reducing edges and $O(n^3)$ for reducing triangles, potentially reducing the memory requirement by a factor of n .

Algorithm 2 Do not store R^\perp : Implicitly compute from V^\perp

```

1: Input:  $F_1$ 
2:  $V^\perp, p^\perp$  are empty
3: for  $e$  in  $F_1^{-1}$  do
4:    $r \leftarrow \delta e$ 
5:    $\delta_* \leftarrow \text{low}(r)$ 
6:    $v \leftarrow [e]$ 
7:   while  $\delta_*$  is not empty AND there is a pair  $(\delta_*, e')$  in  $p^\perp$  do
8:     for  $e''$  in  $V^\perp(e')$  do
9:        $r \leftarrow r \oplus \delta e''$ 
10:     $\delta_* \leftarrow \text{low}(r)$  ▷ Update the low
11:     $v \leftarrow v \oplus V^\perp(e')$  ▷ Update reduction operations for  $e$ 
12:   if  $\delta_*$  not empty then
13:      $V^\perp(e) \leftarrow v$ 
14:      $p^\perp \leftarrow (\delta_*, e)$ 

```

4.3.2 Implicit Row Algorithm

The reduction of the coboundary of an edge requires the computation of the smallest triangle in r with non-zero coefficient, denoted by δ_* in the algorithm. Implicitly, δ_* is the smallest triangle with non-zero coefficient after coboundaries of all edges in the corresponding v are summed. The idea behind the algorithm is that we will store ϕ -representations of only the smallest triangle with non-zero coefficient in the coboundary of every edge in v , the function `FindGEQt` will optimize reduction by eliminating certain redundant reductions, and the function `FindNextt` will traverse along the coboundaries during reduction. We begin with introducing a basic strategy to compute δ_* in this algorithm. To explain the algorithm, we will walk through an example that reduces $r = \delta e_0$ with R^\perp using only v , V^\perp , and p^\perp .

Step 1 (‘initialize’ in Figure 9): As shown in the figure, δ^0 is the smallest simplex in δe_0 . Then, v is initialized as a list with the single entry of ϕ -representation of δ^0 in δe_0 , denoted by $\phi_{e_0} = (e_0, i_a, i_b, \delta^0)$. This corresponds to the information that $r = \delta e_0$ initially and the smallest triangle in r is δ^0 . Subsequently, δ_* is initialized with δ^0 .

Step 2 (‘append’ in Figure 9): Now, suppose there exists a pair (δ_*, e') in p^\perp and $V^\perp(e') = [e'_1, e'_2, e'_3]$. Then, r is to be summed with $R^\perp(e')$. Since the smallest triangle with non-zero coefficient in $R^\perp(e')$ is δ_* , we know that when coboundaries of all e'_k in $V^\perp(e')$ are summed with each other, then every triangle that is smaller than δ_* will have a zero coefficient (shown as shaded area in the figure). Hence, triangles in $\delta e'_k$ that are smaller than δ_* will have zero coefficient and they do not matter. Therefore, for every edge e'_k in $V^\perp(e')$ and the edge e'_0 , we use `FindGEQt` to compute the smallest triangle in their coboundary that is greater than or equal to δ_* , and append its ϕ -representation to v (see (0) in Figure 9). This eliminates unnecessary reductions of the coboundaries of the new edges that are being appended to v . Moreover, `FindGEQt` does so efficiently by considering three cases and conducting binary searches as explained in 4.2.1. Hence, paired-indexing not only improves the limits on memory requirements, but also plays a crucial role in reducing the computation time of the reduction. The updated v corresponds to the updated $r \leftarrow r \oplus R^\perp(e')$, therefore the coefficient of δ_* will be 0. To find the smallest triangle with non-zero coefficient in r , we go to step 3.

Step 3 (‘reduce’ in Figure 9): We first define $\delta = \text{MAX} = \langle n_e, 0 \rangle$ (since $k_1 < n_e$), and then we process every $\phi_e = (e, i_a, i_b, \delta_e)$ in v as follows. If $\delta_e = \delta_*$, then we find the next simplex greater than δ_e in coboundary of e using `FindNextt` since the coefficient of δ_* is 0. If the updated δ_e is less than δ , then we set $\delta \leftarrow \delta_e$ and set the coefficient to 1, otherwise, 1 is added (modulo 2) to the coefficient. As a result, δ stores the smallest triangle greater than δ_* in r , and we also keep track of its coefficient. For example, starting at (0) in Figure 9, $\delta_e = \delta_1$ for the edges e'_3, e'_2, e'_1 , and e_0 . For these edges we compute the next greater triangle in their respective coboundary using `FindNextt`. After iterating through all entries in v , it is determined that δ^1 is the smallest simplex greater than δ_* , and it has a coefficient of 0 (see (1) in figure). We update $\delta_* \leftarrow \delta^1$ and $\delta \leftarrow \text{MAX}$, and we iterate through all entries in v as done previously. In (3)

we get $\delta_* = \delta^2$ with non-zero coefficient. This signals the end of implicit reduction of r with $R^\perp(e'_0)$. To determine whether r is to be reduced with another column of R^\perp , we check if there exists a persistence pair (δ_*, e'') in p^\perp and go back to step 2 to append $V^\perp(e'')$ to v . Otherwise, r is completely reduced and we go to the next step to update p^\perp and V^\perp . In general, it is possible that δ_* is empty, in which case r was reduced to $\mathbf{0}$ and reduction ends without requiring any update to p^\perp and V^\perp .

Step 4 ('update' in Figure 9): If δ_* is not empty, then we add the persistence pair (δ_*, e_0) to p^\perp . To update V^\perp , we first sum all ϕ_e modulo 2. This is because a ϕ_e with zero coefficient implies that the entire coboundary of e will sum to 0 when coboundaries of all edges in v are summed. For every ϕ_e with non-zero coefficient, except for ϕ_{e_0} , we append e to the column $V^\perp(e_0)$. The edge e_0 is not appended to $V^\perp(e_0)$ because ϕ_{e_0} will always have a coefficient 1 and we already store e_0 in the persistence pair (δ_*, e_0) . If the resulting $V^\perp(e_0)$ is empty, then we do not make any record of it. This concludes the complete reduction of r with R^\perp .

There are two pitfalls in the above strategy. First, if an edge e_i occurs an even number of times in v (has zero coefficient in v), then we know that its coboundary will sum to 0 after complete reduction of r , and hence, calling `FindNextt` for each of the multiple entries of e_i during reduction is redundant. The above algorithm trades the cost of computation of coefficient of edges in v with the cost of computing coboundaries. This might be inefficient if there are many edges that sum to 0 in v . Second, computation of δ_* requires traversal across all entries of v at every step of reduction. This does not scale well if r requires a lot of reductions and the corresponding v has a large number of edges. We show next that both of these can be addressed simultaneously when iterating over v during reduction if we ensure that ϕ -representations in v are always ordered appropriately. Further, we will use paired-indexing to optimize it, making it an efficient strategy in terms of both memory requirement and computation time taken.

4.3.3 Implicit Column Algorithm

Alternatively, we can view the ϕ -representations in v as a column of entries ordered first by the lows (δ_i) and by the edges (e_i) for the same lows (see Figure 10). We say that v is ordered by (low, edge). Then, entries in v that correspond to the same lows or that correspond to the same lows in the coboundaries of the same edges, are adjacent to each other. As we move along v , we sum adjacent entries and update the coefficient accordingly. For every ϕ_i in v , we define a flag-next, denoted by f_n^i , that is flagged if the next triangle in the coboundary of the corresponding edge has to be computed and inserted in v . We explain the algorithm below that can address the two pitfalls of implicit row algorithm. The flowchart is shown in Figure 10.

The first two steps of 'initialize' and 'append' are similar to 4.3.2 with two distinctions—new entries are inserted in v such that it is ordered by (low, edge) and the flag-next of every new entry is initialized with 1. To reduce v , we move along it linearly using a pointer, shown in red in Figure 10. It is initialized to point to the first index of v . The only entry in v initially is $(e_0, i_a, i_b, \delta_0)$, hence, `coeff` is initialized to 1 and $\delta_* = \delta_0$. Suppose we point at index i of v at the beginning of a reduction step. The `coeff` then has the coefficient of the entry at index i . To compute δ_* (as defined in implicit row algorithm), we compare the adjacent entries in v and update the coefficient. If $\delta_i = \delta_{i+1}$, then the coefficient is summed by 1 (modulo 2). Additionally, if e_i is also equal to e_{i+1} , we unflag f_n^i and f_n^{i+1} if both are flagged. This eliminates edges e_i and e_{i+1} from subsequent computation of δ_* , which is justified since coboundaries of equal edges will always sum to 0—resolving the first pitfall discussed in 4.3.2. Now, if f_n^i is flagged, we compute $\phi'_i = \text{FindNextt}(\phi_i)$, unflag f_n^i , and insert ϕ'_i in v . It is known that the index of ϕ'_i in v will be strictly greater than i since it has a greater low than ϕ_i . So, the insertion of an element in v does not affect v up to and including index i , and we can by incrementing i by 1. Otherwise, if $\delta_i \neq \delta_{i+1}$, we look at the coefficient. If `coeff` = 1, then δ_i has non-zero coefficient and, hence, $\delta_* = \delta_i$, and we are done with reduction. On the other hand, the value 0 of `coeff` implies that δ_i has 0 coefficient. To proceed, we insert `FindNextt`(ϕ_i) in v if f_n^i is flagged, and we unflag f_n^i . Additionally, we reset `coeff` to 1 to indicate that the smallest triangle with non-zero coefficient is now δ_{i+1} . Then, we increment i by one to continue computation of δ_* . A value of 0 for the coefficient of the last entry in v implies that r is reduced to $\mathbf{0}$.

In implicit row algorithm, it was a requirement to traverse through entire v every time the coefficient of δ_* is 0. In implicit column algorithm also we have to traverse through v to maintain the order of the entries, but this traversal is not necessarily across all v . This potential improvement in computational efficiency is then canceled by the fact that the traversal in implicit column algorithm has to be done every time `FindNextt` is called and a new entry is inserted in v . Further, since we insert entries in v in implicit column algorithm in contrast to replacing them in implicit row algorithm, the size of the data structure that stores v is theoretically bounded by the size of r . As a result, this algorithm is not practically feasible yet, and in the next section we will show next how paired-indexing will solve both of these issues.

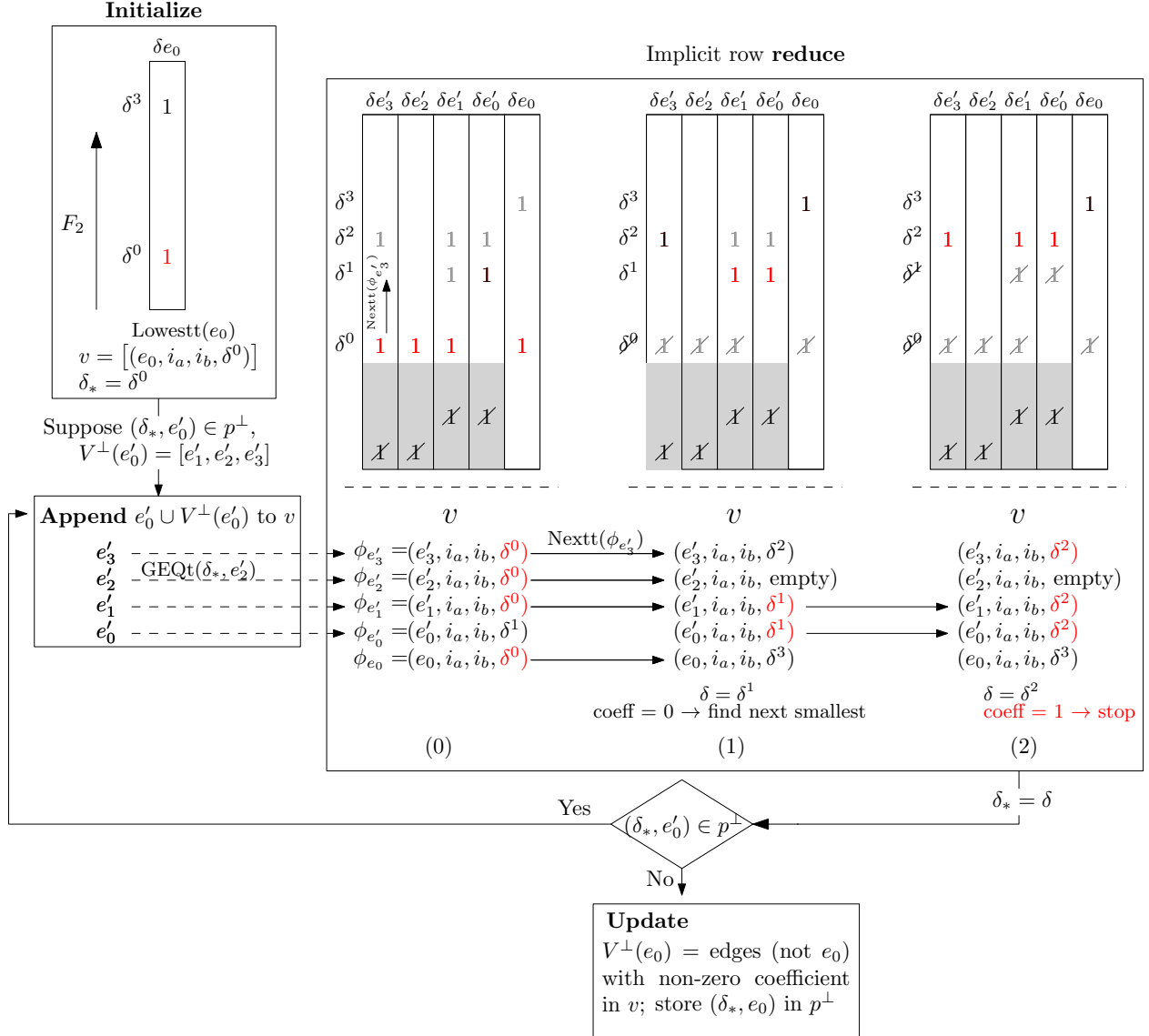


Figure 9: Example to show implicit reduction of $r = \delta e_0$ with R^\perp using V^\perp and p^\perp . For every edge in v , we record the smallest triangle in its coboundary with non-zero coefficient using the ϕ -representation (marked in black). The smallest among these are marked in red. Simplices with zero coefficient are shown as crossed out.

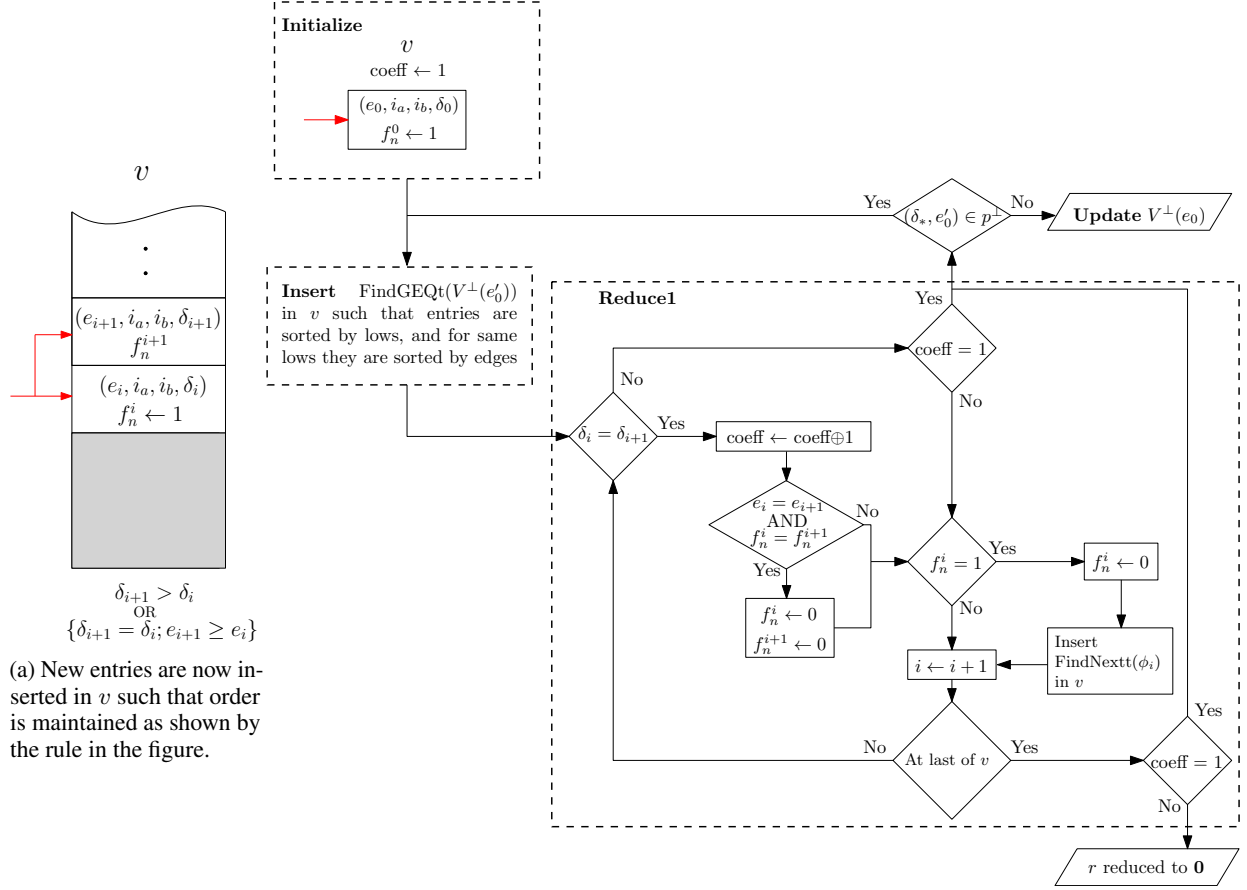
(b) Flowchart to compute δ_* with non-zero coefficient.

Figure 10: Implicit column algorithm.

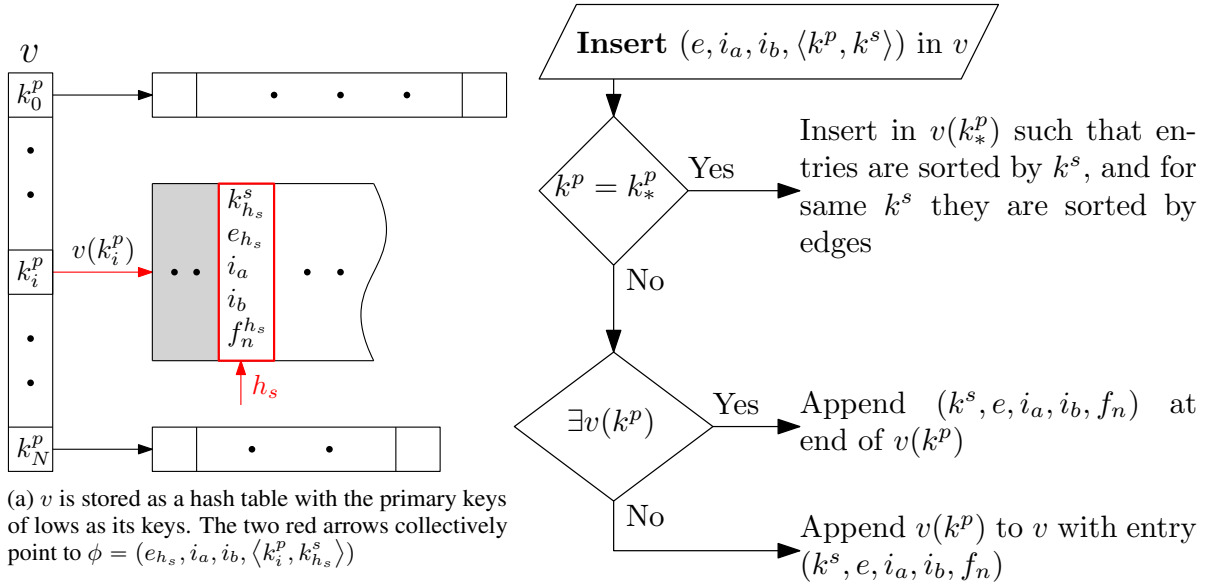
(b) Flowchart for inserting new entries in the hash table of v .

Figure 11: Fast implicit column algorithm, using paired-indexing to make a hash table.

4.3.4 Fast Implicit Column Algorithm

To efficiently compute $\delta_* = \langle k_*^p, k_*^s \rangle$, the smallest triangle with non-zero coefficient, we first observe that it will have the smallest primary key among all lows in v . Now, using paired-indexing, we can store v as a hash table that is defined by a list of unique primary keys that are in the lows of the entries in v , and each entry in this list is mapped to a list of lows in v that have the same primary key. Figure 11a shows an example of such a hash map. The keys of this hash table are stored as a linear list of primary keys $[k_i^p]$ (in no particular order), and each primary key is mapped to a linear list $v(k_*^p)$, with elements of the form (k^s, e, i_a, i_b, f_n) . In Figure 11a, the entry in the red box is at index h_s of $v(k_i^p)$, and it corresponds to $\phi = (e_{h_s}, i_a, i_b, \langle k_i^p, k_{h_s}^s \rangle)$ with the corresponding flag-next $f_n^{h_s}$.

To compute δ_* using this hash table, we first find the primary key with the smallest order, denoted by k_*^p , and then compare adjacent entries in $v(k_*^p)$ (see flowchart in Figure 12). That is why, the entries in $v(k_*^p)$ have to be ordered by secondary key and those with same secondary key have to be ordered by the edge. We denote this ordering by (secondary key, edge). Note that, the order of elements of $v(k^p)$ for $k^p \neq k_*^p$ does not matter. To ensure this, we define the insertion of a new entry in this hash table as follows (see Figure 11b). Suppose the new entry to be inserted is $(e, i_a, i_b, \langle k^p, k^s \rangle)$. If $k^p = k_*^p$, then $(k^s, i_a, i_b, f_n = 1)$ is inserted in $v(k_*^p)$ such that its entries are ordered according to (secondary key, edge). Otherwise, we check whether k^p exists in the list of keys of the hash table. If true, we append $(k^s, i_a, i_b, 1)$ to the end of $v(k^p)$ since the order of its entries does not matter. If $v(k^p)$ does not exist, then we append k^p to the list of keys of the hash table, and we map $v(k^p)$ to a list with a singular entry of $(k^s, i_a, i_b, 1)$. In this strategy, it is not required for entries in $v(k^p)$ to be in a specific order when $k^p \neq k_*^p$, and we also do not maintain the order of the list of keys of the hash table. Hence, we maintain the order only of the entries that are crucial for computation of δ_* , that is, precisely those that have the primary key as the smallest key of the hash table in the current reduction iteration. This optimizes the computational overhead of maintaining the order during insertion of new entries in v .

Now, if h_s reaches the last entry of $v(k_*^p)$, it does not imply that we have reached the last entry of the hash table, and we proceed as follows. If $\text{coeff} = 1$, then $\delta_* = \langle k_*^p, k_{h_s}^s \rangle$ and we are done. Otherwise, if $\text{coeff} = 0$, then we first check whether $f_n^{h_s}$ flagged. If it is flagged, we compute $(e_{h_s}, i_a, i_b, \langle k_{\#}^p, k_{\#}^s \rangle) = \text{FindNextt}((e_{h_s}, i_a, i_b, \langle k_*^p, k_{h_s}^s \rangle))$ and insert it in the hash table. If $k_{\#}^p = k_*^p$, then $(k_{\#}^s, e, i_a, i_b, 1)$ is the last entry in the updated $v(k_*^p)$, and also, h_s does not point to the last entry in $v(k_*^p)$. We know that the next simplex in δe_{h_s} will be greater than $\langle k_{\#}^p, k_{\#}^s \rangle$, hence, it is not required to compute FindNextt again, and $\langle k_{\#}^p, k_{\#}^s \rangle$ will have a coefficient of one. So, $\delta_* = \langle k_*^p, k_{h_s+1}^s \rangle = \langle k_{\#}^p, k_{\#}^s \rangle$ and we are done. Otherwise, if $k_{\#}^p \neq k_*^p$ or if $f_n^{h_s}$ was unflagged, we have traversed through all entries in $v(k_*^p)$ and we mark the memory occupied by $v(k_*^p)$ as free space that can be overwritten. As a result, the memory used by the hash table will never approach r , addressing the second pitfall discussed in 4.3.3. To proceed, we iterate through rest of the keys of the hash table (that are not empty) and update k_*^p with the smallest primary key. Since $v(k_*^p)$ might not be sorted, we first sort it by (secondary key, edge). Then, we update $h_s \leftarrow 0$ and $\text{coeff} \leftarrow 1$, and we proceed with the computation of δ_* . If there are no keys left in the hash table, then r was reduced to 0.

The fast implicit column algorithm to compute H_2^* similarly uses paired-indexing along with the ϕ -representation for tetrahedrons introduced in Section 4.2.2 and the functions FindSmallesth , FindNexth , and FindGEqh . It scales more efficiently than the implicit row algorithm. See 4 in appendix E for a comparison between the two algorithms for test data sets that are used for benchmarking in this study (Section 5).

4.3.5 Trivial Persistence Pairs

For further reduction in memory usage, we notice that there are specific persistence pairs that can be computed on the fly and do not require storage in p^\perp . Figure 13 shows an example of coboundary matrices for edges and triangles. The triangle $t = \langle ab, c \rangle$ will be in the coboundary of exactly three edges (see Figure 13a). Since the diameter of t is $\{a, b\}$, the row of t will have all zeroes to the left of $(\langle ab, c \rangle, ab)$. If additionally, t is the smallest simplex in the coboundary of $\{a, b\}$, then there will be all zeroes below $(\langle ab, c \rangle, ab)$. Consequently, $(\langle ab, c \rangle, ab)$ will be a persistence pair and will not require any reduction. We will call such pairs *trivial persistence pairs*, and we will not store them in p^\perp . Instead, during the reduction of r , we check whether $\delta_* = \langle k_1, k_2 \rangle$ is the smallest simplex in the coboundary of the edge $e' = f_1^{-1}(k_1)$. If true, then (δ_*, e') is a trivial persistence pair and the next reduction is to be with exactly the coboundary of e' (since trivial persistence pairs do not require any reductions). Conducting this check at every step of reduction is computationally feasible because paired-indexing gives direct access to the diameter of t , making these checks inexpensive. For further optimization, the smallest simplex in the coboundary of each edge is stored a priori at the cost of $O(n_e)$ memory.

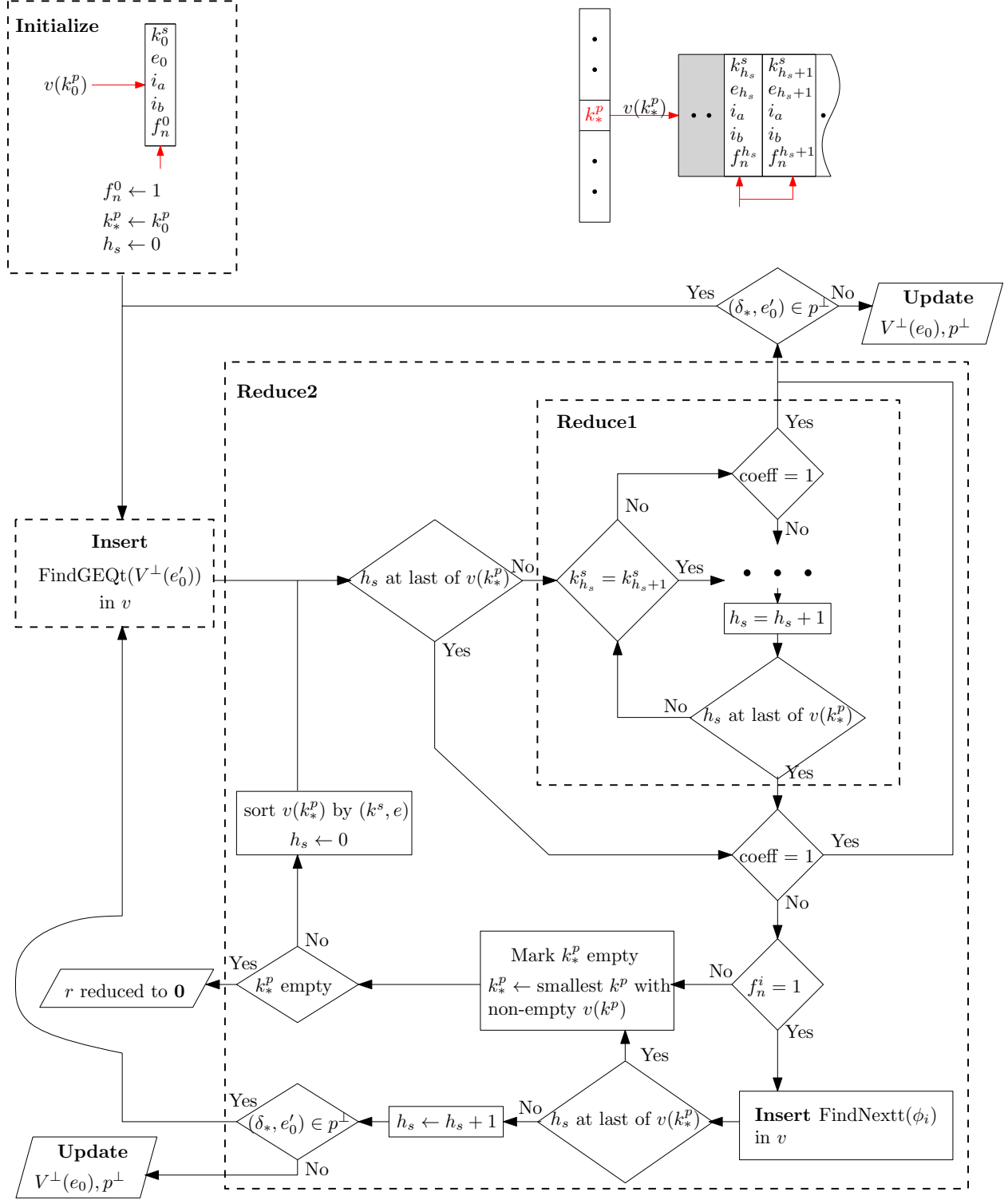


Figure 12: Flowchart for fast implicit column algorithm in which v is stored as a hash table using paired-indexing. The three dots in box ‘Reduce1’ denote that it is similar to the flowchart in Figure 10b.

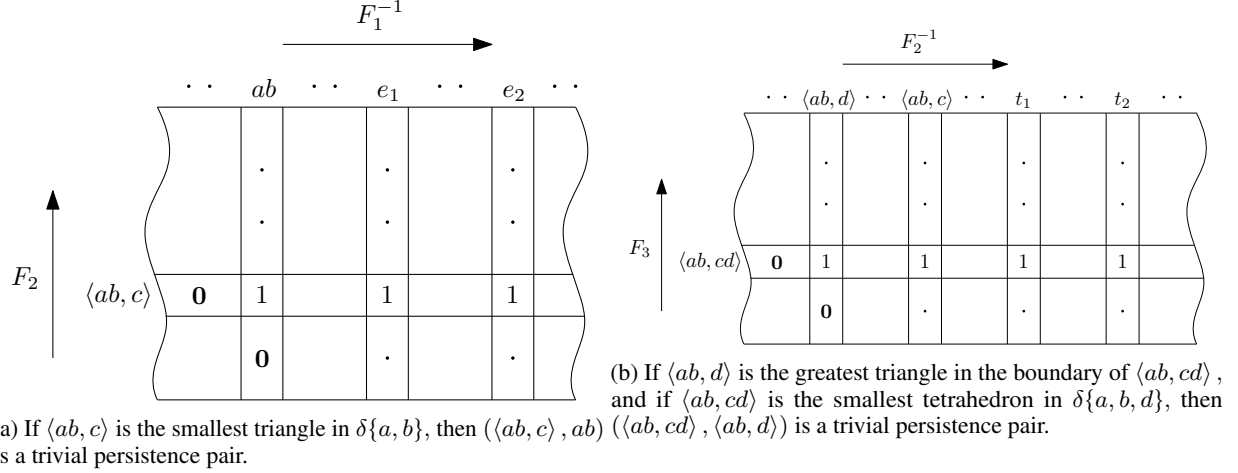


Figure 13: Trivial persistence pairs

Similarly, a tetrahedron, $h = \langle ab, cd \rangle$, will be in the coboundary of exactly four triangles (see Figure 13b). The greatest triangle in the boundary of h will be $t = \langle ab, \max\{c, d\} \rangle$. Following similar reasoning, if h is the smallest simplex in the coboundary of t , then we say that (h, t) is a trivial persistence pair. During reduction of any triangle, we check whether $\delta_* = \langle k_1, k_2 \rangle$ is the smallest simplex in the coboundary of the triangle $t' = \langle k_1, \max\{f_1^{-1}(k_2)\} \rangle$. If true, (δ_*, t') is a trivial persistence pair and the next reduction is to be with the coboundary of t' . `FindSmallesth` is used to check whether δ_* is the smallest simplex in $\delta t'$.

4.4 Parallelizing: A General Serial-parallel Reduction Algorithm

To reduce the computation time required to process the large number of simplices in the VR-filtration, we developed a novel serial-parallel algorithm that can reduce multiple simplices in parallel. In essence, rather than reducing one simplex at a time, we will reduce a batch of simplices. Any algorithm cannot be embarrassingly parallel because of the inherent order in reduction imposed by the filtration. We introduce the serial-parallel algorithm by parallelizing the standard column algorithm (algorithm 1) for cohomology computation (see Figure 16).

Parallel (Figure 14a): Suppose R^\perp contains reductions of the first n edges in F^{-1} . Let $\mathbf{r} = [r_1, \dots, r_B]$ be the batch of next B edges in F_1^{-1} that have to be reduced. Initially, each r_i is the coboundary of the corresponding edge, and during reduction it contains the result of the ongoing reduction. Then, if the low of r_i and r_j in \mathbf{r} is equal to that of $R^\perp(e)$ for some edge e , reducing r_i and r_j with $R^\perp(e)$ will take precedence over reducing them with each other. As a result, each r_i can be reduced with R^\perp in parallel.

Serial (Figure 14b): After \mathbf{r} has been reduced with R^\perp , we reduce the columns in \mathbf{r} with each other using *serial reduction*. We ‘mark’ r_i if it is completely reduced. After parallel reduction, none of the r_i have the same low as any column in R^\perp . Hence, r_1 is completely reduced and we mark it. Then, carrying out the standard column algorithm, the low of every r_i ($i > 1$) is compared sequentially with r_j for every $j < i$. We consider the following cases for every r_j . (1) If $\text{low}(r_j) > \text{low}(r_i)$, then we skip it. (2) Otherwise, we check whether r_j is marked. (2a) If it is unmarked, we cannot continue reduction of r_i before reducing r_j so we unmark r_i and increment i by one. (2b) If r_j is marked and $\text{low}(r_j) = \text{low}(r_i)$, then we reduce r_i with r_j , and we check whether the new low of r_i is also the low of a column in R^\perp . If true, then r_i has to be reduced with R^\perp before reducing with any r_j in \mathbf{r} , and we unmark r_i and increment i by one. Otherwise, if the updated low is not the low of any column in R^\perp , then $j \rightarrow 1$. This process is repeated to reduce r_i until either j reaches i or r_i is unmarked. When all of \mathbf{r} has been processed, that is, i reaches the end of \mathbf{r} , we go to clearance. A detailed hypothetical example is shown in Figure 15.

Clearance: All marked r_i are appended to R^\perp , freeing up space in \mathbf{r} to be filled in by the coboundaries of the next edges from F_1^{-1} . After filling \mathbf{r} with the new coboundaries, we go back to parallel reduction. This process is continued until all edges in F_1^{-1} have been reduced. The structure of the algorithm is shown in Figure 16.

In Dory, we implement the serial-parallel algorithm to compute H_0 , H_1^* , and H_2^* . We discuss the implementation for cohomology computation in detail. The batch to be reduced is represented by $\mathbf{v} = [v_1, \dots, v_B]$, and we store V^\perp and p^\perp . Then, reducing r_i with R^\perp is implemented using the fast implicit column algorithm using v_i and V^\perp , as shown

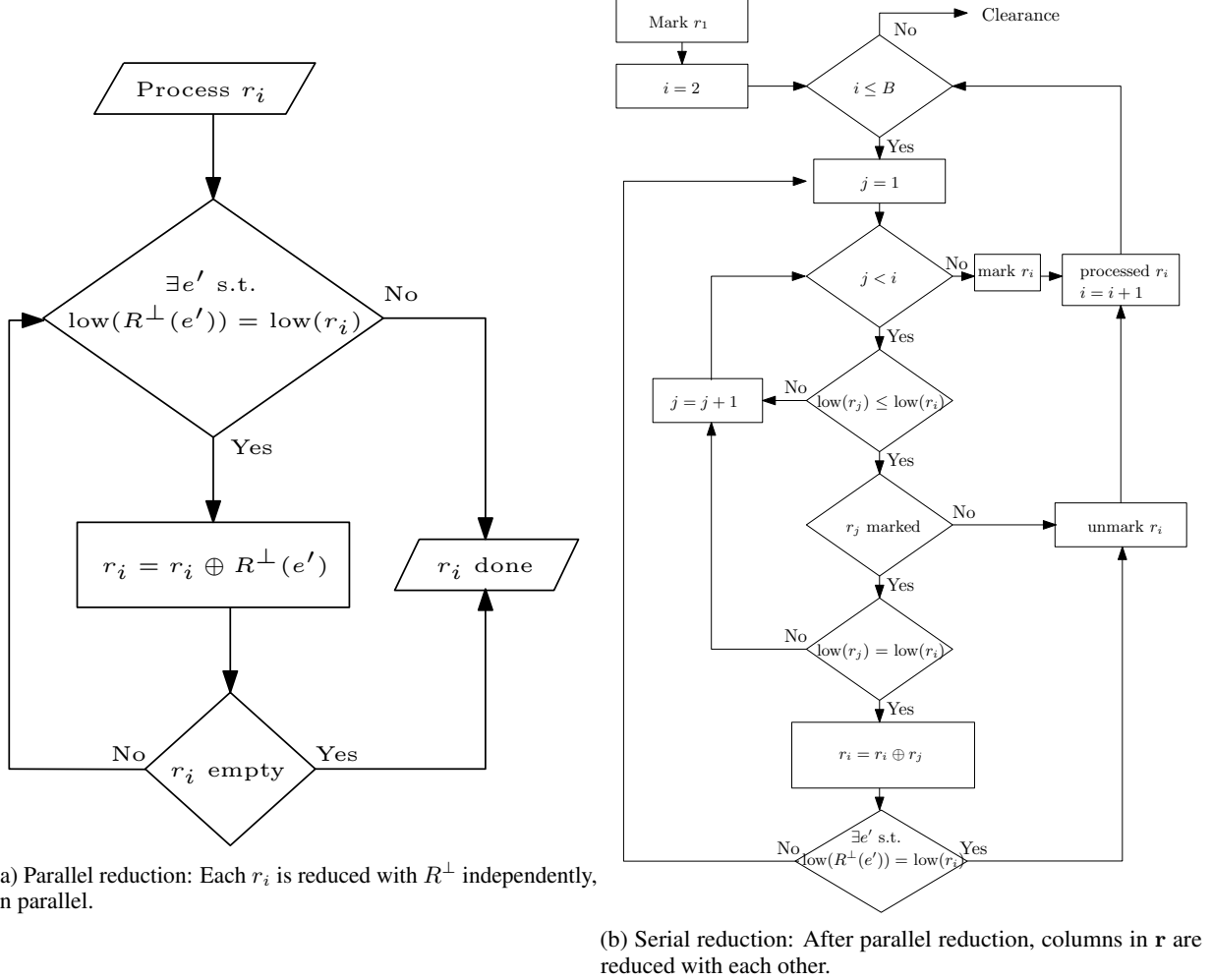


Figure 14: Flowcharts for parallel and serial reductions that form the serial-parallel algorithm.

earlier. The implicit reduction of r_i with r_j using v_i and v_j is modified slightly because v_j stores the ϕ -representations and `FingGEQh` is not required when appending v_j to v_i . Suppose k_{j*}^p is the smallest primary key in v_j and h_s^j is the index in $v(k_{j*}^p)$ that points to the smallest low with non-zero coefficient. Then, merging v_i with v_j is done by inserting every entry of v_j in v_i , except for the entries that are in $v(k_{j*}^p)$ before the index h_s^j . Additionally, trivial persistence pairs are not stored and are computed on the fly in the parallel reduction. The modified flowcharts are shown in Figure 17. For different scenarios during serial reduction, we use four different flags for every r_i — f_v flags whether r_i has to be reduced with a trivial persistence pair; f_r flags whether r_i is to be reduced with R^\perp ; f_a is flagged if it is completely reduced; and f_e is flagged if r_e is empty. Note that flagging f_v and f_r is similar to unmarking r_i , and flagging f_a is similar to marking r_i . The basic flow of the serial-parallel algorithm to reduce triangles is shown in algorithm 16. See appendix D for pseudocode of serial (algorithm 18) and parallel (algorithm 17) reduction. The default value of the batch-size for serial-parallel implementation of H_2^* computation is chosen as 100 and for H_0 it is 1000. These hyperparameters can be optimized for any data set. A smaller value of batch-size can increase the computation time by lowering the number of simplices that are reduced in parallel, but a larger value of batch-size can increase the computation time spent in the serial reduction. The parallelized section of the serial-parallel algorithm will be called many times in the serial-parallel reduction. To reduce the overhead of creating and destroying threads, we create threads before the computation of PH. The jobs are allocated in fixed chunks to these threads and the threads are woken up when they are required and destroyed after computation of PH. We use light-weight POSIX threads, or pthreads.

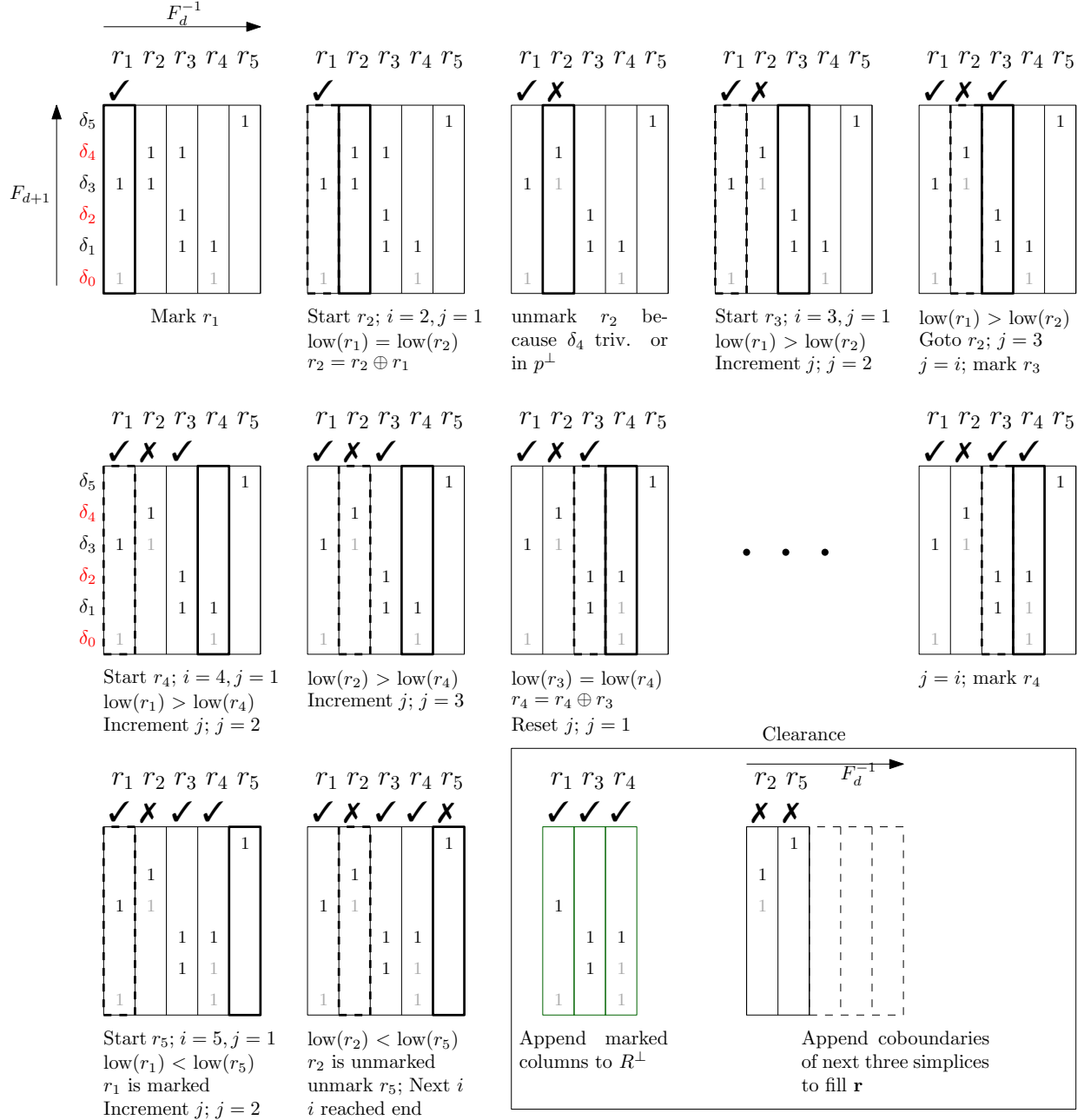


Figure 15: Hypothetical example to illustrate serial reduction in serial-parallel algorithm. The simplices marked by red indicate that they are in a persistence pair in p^\perp .

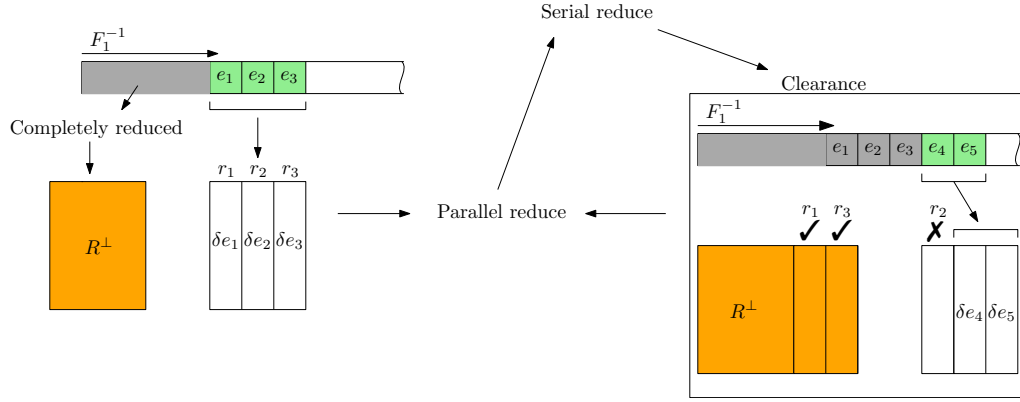
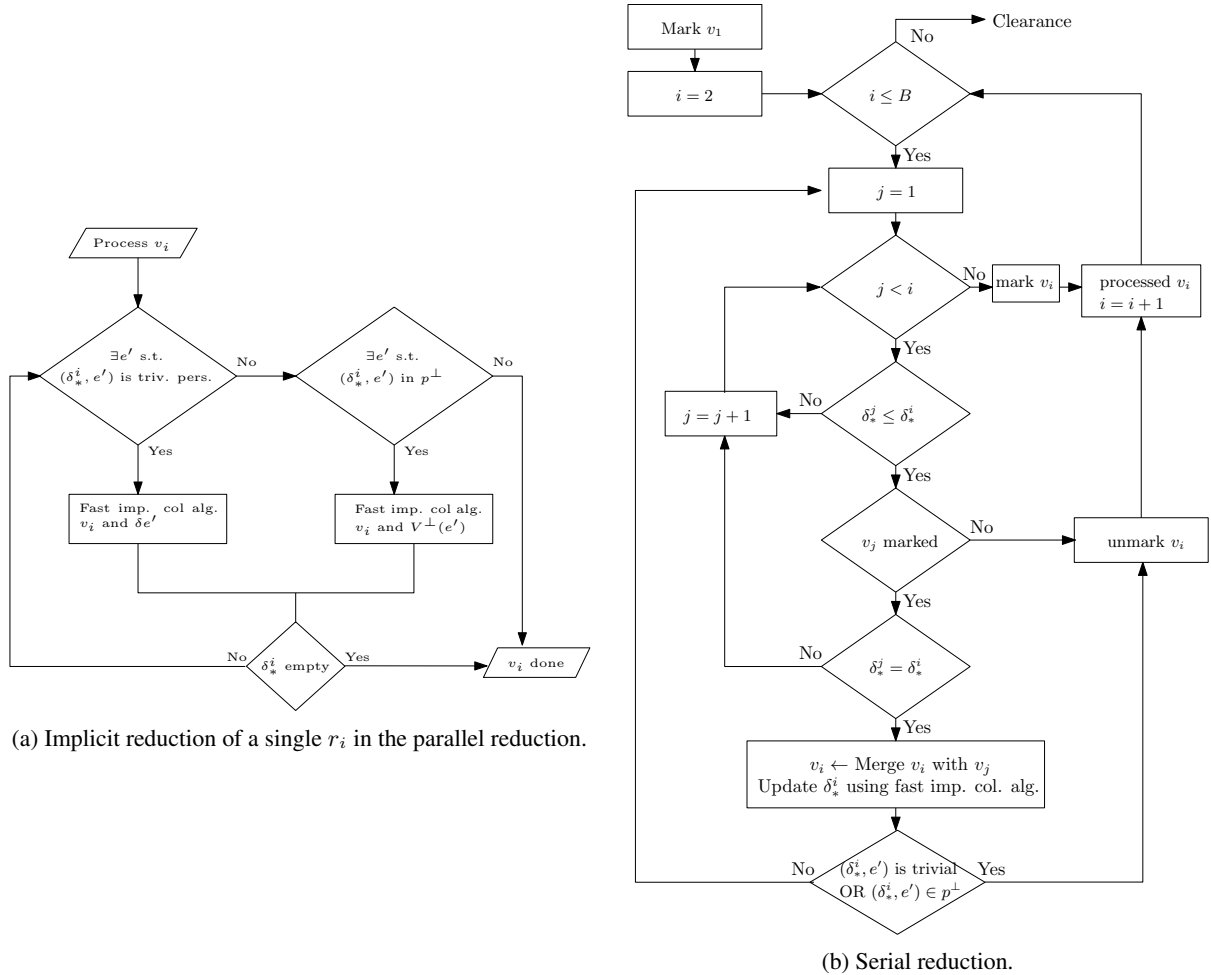


Figure 16: Serial-parallel algorithm to reduce coboundaries of edges. Similar algorithm structure is used to parallelize reduction of coboundaries of edges (H_1^*) and triangles (H_2^*) and to reduce boundaries of edges (H_0).



(a) Implicit reduction of a single r_i in the parallel reduction.

(b) Serial reduction.

Figure 17: Flowcharts for algorithms in serial-parallel reduction using fast implicit column algorithm and incorporating trivial persistence pair computation.

Data set	n	τ_m	n_e	d	N
dragon	2000	∞	1999000	1	1333335000
fractal	512	∞	130816	2	2852247168
o3	8192	1	327614	2	33244954
torus4(1)	50000	0.15	2242206	1	41629821
torus4(2)	50000	0.15	2242206	2	454608895
Hi-C (control)	3087941	400	51233398	2	110946257
Hi-C (auxin)	3087941	400	35170863	2	36012219

Table 1: Data sets used for benchmarking in this study.

4.5 All Together with Clearing Strategy

We summarize the algorithm to compute the persistence pairs for groups H_0 , H_1^* , and H_2^* in algorithm 3, including the clearing strategy suggested by Chen and Kerber [2011]. This strategy provides significant reduction in computation time of cohomology reduction by eliminating the need for reduction of certain simplices. In essence, if (τ, σ) is a persistence pair in H_d (or (σ, τ) is in H_d^*), then there cannot exist a persistence pair (σ, ω) in H_{d+1} . Consequently, there cannot exist a pair (ω, σ) in H_{d+1}^* , and there is no need to reduce the coboundary of σ when computing H_{d+1}^* .

Algorithm 3 Computing all

```

1: Input:  $F_1$ 
2: Output: Persistence pairs in  $H_0, H_1^*, H_2^*$ 
3:
4: for  $e$  in  $F_1$  do ▷ Compute  $H_0$ 
5:   Serial-Parallel reduction
6:
7: for  $e$  in  $F_1^{-1}$  do ▷ Compute  $H_1^*$ 
8:   if  $e$  is in a persistence pair in  $H_0$  then ▷ Clearing strategy
9:     continue
10:   Reduction
11:
12: for  $e$  in  $F_1^{-1}$  do ▷ Compute  $H_2^*$ 
13:   for  $t$  in  $\delta e$  with  $d(t) = e$  do
14:     if  $t$  is in a persistence pair in  $H_1^*$  then ▷ Clearing strategy
15:       continue
16:   Serial-parallel reduction

```

4.6 Sparse vs. Non-Sparse

In the case of non-sparse filtrations, our experiments showed that most of the computation time was being spent on the binary searches in edge- and vertex-neighborhoods to find orders of the edges during cohomology computation. We implemented an alternate version in which we use combinatorial indexing to store the orders of all edges in the filtration. This reduces computation time by replacing binary search by an array access at the cost of using $O(n^2)$ memory instead of $O(n_e^2)$. We call the non-sparse version DoryNS. In most cases it is advisable to use Dory because the reduction in peak memory usage outweighs the computation cost. DoryNS should be considered when computing H_2 for non-sparse filtrations.

5 Computation and Benchmarks

We tested Dory with six data sets—dragon, fractal, o3, torus4, Hi-C control, and Hi-C auxin (Table 1). The data sets dragon and fractal were used in Otter et al. [2017] to benchmark PH algorithms, o3 and torus4 are taken from the repository of Ripser [Bauer, 2019], and the Hi-C data sets are from Rao et al. [2017]. They are briefly described as follows—dragon is a point-cloud in 3-dimensional space; fractal is the distance matrix for nodes in a self-similar network; o3 consists of 8192 random orthogonal 3×3 matrices, that we consider as a point-cloud in nine dimensional

Data set	Creating F_1	Creating N^v, E^v	H_0	H_1^*	H_2^*
dragon	1.14	0.488	0.144	0.36	NA
fractal	0.09	≈ 0	0.01	0.03	30.5
o3	0.4	0.03	0.03	1.4	2.9
torus4	5.74	0.66	0.25	1.95	30.68
Hi-C (control)	26.47	17.29	41.17	106.98	68.94
Hi-C (auxin)	17.64	10.29	21.57	20.35	15

Table 2: Time taken in seconds for different processes in Dory (4 threads and without `-D PRINT` compiler flag so that it does not print the persistence pairs in the terminal window).

Data set	Ripser	Dory		DoryNS	
		4 thds.	1 thd.	4 thds.	1 thd.
dragon	(2.57 s, 199 MB)	(2.8 s, 262 MB)	(3.3 s, 270 MB)	(3.16 s, 277 MB)	(3.59 s, 269 MB)
fractal	(7.54 s, 775.13 MB)	(31.9 s, 695 MB)	(40.5 s, 687 MB)	(21.6 s, 810 MB)	(23.8 s, 802.8 MB)
o3	(6.47 s, 219 MB)	(5.07 s, 157 MB)	(6.43 s, 149 MB)	(4.86 s, 285 MB)	(6.2 s, 277 MB)
torus4(1)	(31.54 s, 12 GB)	(8.83 s, 328 MB)	(10.9 s, 321 MB)	(11.7 s, 5 GB)	(13.6 s, 5 GB)
torus4(2)	(94 s, 12 GB)	(40.74 s, 1 GB)	(59.3 s, 1 GB)	(42.7 s, 5.7 GB)	(60 s, 5.7 GB)
Hi-C (control)	NA	(276 s, 6.23 GB)	(540 s, 6.21 GB)	NA	NA
Hi-C (Auxin)	NA	(123 s, 3.98 GB)	(230 s, 3.98 GB)	NA	NA

Table 3: Time taken (seconds) was measured using the command `time` in the terminal of macOS. Peak memory usage is recorded using the application Instruments in macOS. The highlighted results indicate efficient performance.

space; torus4 is a point-cloud randomly sampled from the Clifford torus $S^1 \times S^1 \subset \mathbb{R}$; and the two Hi-C data sets are correlations matrices for around three million points (see Section 6 for more details). The benchmarks for PH computation of torus4 data set up to and including H_1^* are shown as torus4(1) and up to and including H_2^* are shown as torus4(2). The data sets can be found at <https://github.com/nihcompmed/Dory>. All computations are done on a computer with a 2.4 GHz 8-Core Intel Core i9 processor and 64 GB memory. We first comment on the computation time and memory taken by Dory.

The computation time taken by Dory can be split into following processes—create F_1 , create the vertex- and edge-neighborhoods, and compute the persistence pairs (see Table 2 for results with Dory using 4 threads). In the dragon data set, almost half of the computation time is spent in creating F_1 . We believe that this can be significantly improved since we call a memory allocation for every edge in the current version of Dory. The other process in Table 2 that takes a significant amount of time is the computation of H_2^* . This follows from the facts that there are generally more simplices to be processed as compared to H_1^* , and that all computations of coboundaries of triangles require binary searches, whereas, computation of coboundary of an edge does not require binary search when in Case 1 (Section 4.2.1). We improved the latter by implementing the non-sparse version, DoryNS at the cost of higher peak memory usage (see Table 3). The former might be improved by determining special classes of persistence pairs a priori [Bauer, 2019] that have been shown to not require any reductions, but their implementation and impact on computational feasibility within Dory’s framework is not yet clear and is an ongoing work.

The memory taken can be split into two parts—the base memory that is used by F_0, F_1 , and the vertex- and edge-neighborhoods, and the PH-memory used for homology and cohomology computations. The practical difference between these is that the base memory is known before computation of PH to be exactly $(3n + 12n_e) \times 4$ bytes in Dory for a data set with n points and n_e permissible edges in the filtration (see appendix E for this calculation), but PH-memory can be significantly more depending upon the reduction operations that need to be stored. Hence, the scaling of PH-memory can decide the feasibility of computation of PH for a data set.

Since Ripser outperforms both Gudhi and Eirene in computing PH for VR-filtrations, we compare time taken and peak memory usage between Dory and Ripser in this section (see Table 3), and the results with Gudhi and Eirene can be found in appendix E. The Ripser source file was downloaded from <https://github.com/Ripser/ripser> and compiled using `c++ -std=c++11 ripser.cpp -o ripser -O3`. DoryNS was compiled using the additional flag `-D COMBIDX`. Both were executed in the terminal of macOS (v 10.15.7). The computation time is the ‘total’ as reported by the command `time` and the peak memory usage was recorded using the application Instruments (v 12.2) in macOS in a separate execution.

We first address the benchmarks in Table 3 in which Ripser does better than Dory. For the dragon data set, Dory is slower than Ripser by ≈ 0.2 s and takes 80 MB more memory. The former can be attributed to the inefficiency of creating F_1 in Dory for which it takes almost half the total runtime for this data set. The higher peak memory usage can arguably be explained by the differences in the base memory because Dory additionally creates vertex- and edge-neighborhoods. However, as the size of the data set increases, the PH-memory will generally define the peak memory usage. For the fractal data set, Dory is slower than Ripser by a factor of 3 because Ripser identifies a large number of simplices that do not require any reduction during H_2^* computation of this data set. Implementation of this strategy in Dory is an ongoing work. DoryNS is faster than Dory, but it is still slower than Ripser for this data set. It is advisable to use Ripser to compute H_2^* for small data sets that are non-sparse.

For larger data sets with sparse filtrations, Dory outperforms Ripser in both computation time and memory taken, and it extends PH computation to data sets with millions of points. For example, to compute persistence pairs for dim-1 for the torus4 data set, Dory takes only 328 MB as compared to 12 GB taken by Ripser, and it is also faster by a factor of 3. To compute persistence pairs up to and including dim-2 for the same data set, Dory takes 1 GB in contrast to 12 GB taken by Ripser, and it is also faster by a factor of 2. To show an application of computing PH of a data set with millions of points, we compute PH up to and including dim-2 for the Hi-C, control and auxin, data sets. These data sets are defined by a distance matrix that is stored in a sparse format. Ripser crashed giving an overflow error, possibly due to combinatorial indexing of tetrahedrons in a data set with millions of points. Ripser-128bit (<https://github.com/Ripser/ripser/tree/128bit>) is an implementation of Ripser that uses 128-bit int, and hence, it is technically able to encode the filtration on these data sets using combinatorial indexing. It did not give an overflow error, but we stopped the simulation after waiting for two hours. Dory, on the other hand, took (276 s, 6.23 GB) for Hi-C control and (123 s, 3.98 GB) for Hi-C auxin data set. Also, Dory performs consistently better with 4 threads across all data sets as compared to one thread, reducing the computation time by up to a factor of 2 for the Hi-C data sets with negligible increase in the peak memory usage.

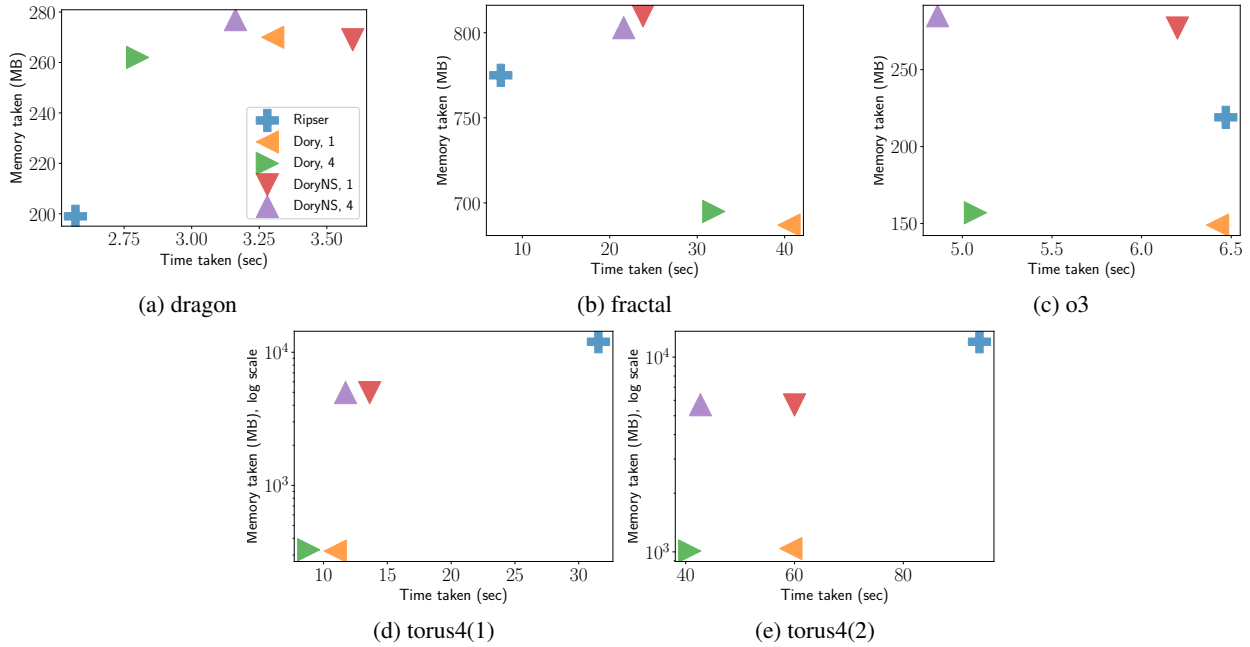


Figure 18: Computation time and peak memory usage by Dory, DoryNS, and Ripser for the data sets used for benchmarking. The peak memory usage for torus4 data set is shown in log scale. Results for Hi-C data sets are not shown here because only Dory was able to process it.

All PDs are shown in appendices F and G. We observed a discrepancy in the PDs of o3 data set for Gudhi (see Figures 19 and 20), specifically in topological features that do not die. The Gudhi PDs were produced using parameters `points = data`, `max_edge_length = 1` in the method `RipsComplex` (Python v 3.8.5). In the resulting file, `inf` entries were replaced by `-1` before plotting. The benchmarking and plotting codes can be found at <https://github.com/nihcompmed/Dory>. We did not explore features of Gudhi, for example, the edge collapse option, that might improve its efficiency or give a consistent PD.

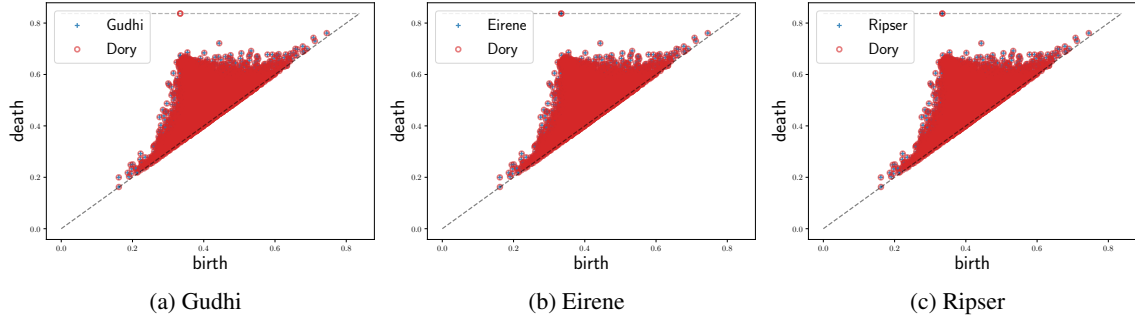


Figure 19: $o_3 H_1$ PD: Gudhi does not report one feature that does not die and is reported by other algorithms.

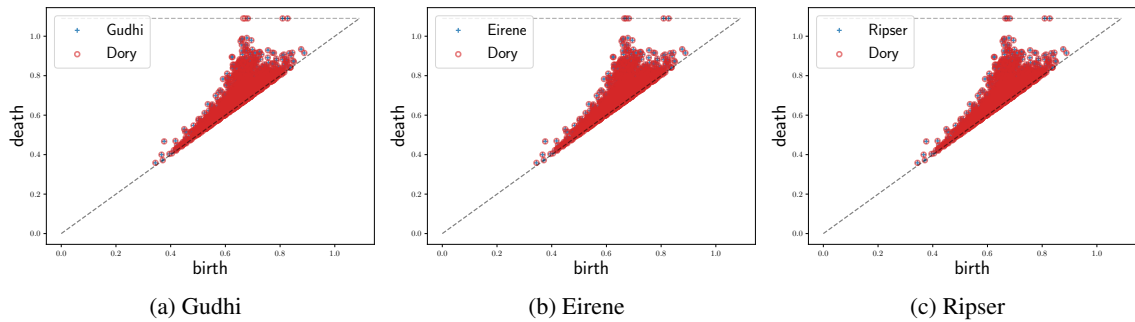


Figure 20: $o_3 H_2$ PD: Gudhi does not report two features that do not die and are reported by other algorithms.

6 Topology of Human Genome

Among different techniques to quantify chromatin structure, Hi-C experiments allow relatively unbiased measurements across an entire genome [Lieberman-Aiden et al., 2009]. Hi-C is based on chromosome conformation capture (3C) which attempts to determine spatial proximity in the cell nucleus between pairs of genetic loci. The experiments measure the interaction frequency of every pair of loci on the genome, and this is believed to correlate with spatial distance in the cell nucleus [Lieberman-Aiden et al., 2009, Dixon et al., 2012].

Using Hi-C experiments, Rao et al. [2014] identified chromatin loops in mouse lymphoblast cells which are orthologous to loops in human lymphoblastoid cells. To highlight the functional importance of chromatin loops they provide multiple sources of evidence that associate most of the detected loops with gene regulation. Rao et al. [2017] showed that treatment of DNA with auxin removes most loop domains.

We test this result by computing PH to compare the number of loops (and voids) across the Hi-C data sets from two different experimental conditions—with and without auxin treatment, provided in Rao et al. [2017]. To compute PH, the DNA is visualized as a point-cloud where each point represents a contiguous segment of a 1000 base pairs on a chromosome, a so-called genomic bin. The relative pairwise spatial distances between genomic bins are then estimated from the Hi-C data set at this 1 kilobase resolution. The functionally significant loops in this point-cloud are most likely the ones with spatially close genomic bins on their boundary to allow for biological interaction via physical processes such as diffusion. Therefore, we compute PH up to a low τ_m resulting in a sparse filtration.

In Figure 21, we plot the percentage change in the number of loops and voids upon addition of auxin ($(\beta_i^{\text{auxin}} - \beta_i^{\text{control}}) / \beta_i^{\text{control}} * 100$). It shows that there is a significant decrease in the number of loops, corroborating previous results [Rao et al., 2017]. The analysis using PH additionally shows that the percentage of reduction in the number of loops is greater for thresholds less than 50 and between 100 and 200, and it also shows that most voids are not born when auxin is added. These results warrant an investigation into possible biological implications. The PDs are shown in appendix G.

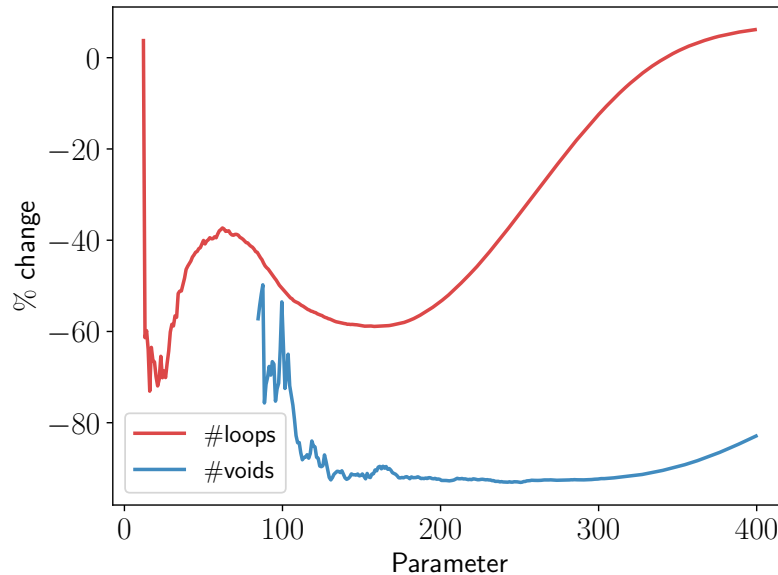


Figure 21: PH of the entire human genome at 1 kilobase resolution shows that the number of loops and voids decreases significantly upon addition of auxin.

7 Discussion

In this paper we introduced a new algorithm that overcomes computational limitations that have prevented the application of PH to large data sets. Compared with pre-existing algorithms, Dory provides significant improvements in memory requirements, without an impractical increase in the computation time. Dory is able to process the large Hi-C data set for the human genome at high resolution, corroborating the expected topology changes of chromatin in different experimental conditions.

While our algorithm is limited to computing PH for VR-filtrations up to three dimensions, a large class of real-world scientific data sets requires only such dimensional restrictions. The current implementation of the algorithm computes PH modulo 2, but it can be easily extended to any prime field.

An alternate class of methods deals with large data sets by approximating their PDs. For example, SimBa [Dey et al., 2019] reduces the number of simplices in the filtration by approximating it to a sparse filtration such that the PDs of the sparse filtration are within a theoretical error of margin when compared to those of the original filtration. Another method, PI-Net [Som et al., 2020], uses neural networks to predict persistence images, that are pixelated approximations of PDs in \mathbb{R}^2 . The former method uses Gudhi to compute PDs of the approximated sparse filtrations and the latter uses Ripser to compute true PDs when training the neural network. Since Dory can handle larger data sets compared to both Gudhi and Ripser, SimBa and PI-Net can expand their scope by using Dory instead.

In this paper we have focused on computing PDs. However, our algorithm can also be extended to compute representative boundaries of the holes and voids in the data set. For scientific applications, these representative boundaries of topological features in the data set are critical for connecting topology to structural properties of the data that may be linked to functional properties of the underlying system. For instance, they might yield insights into the biological implications of a reduction in the number of voids in human genome upon treatment with auxin. Computation of representative boundaries faces the hurdle of high memory cost. We are currently working on developing a scalable algorithm.

Acknowledgement

This research was supported by the Intramural Research Program of the NIH, the National Institute of Diabetes and Digestive and Kidney Diseases (NIDDK).

Appendices

A Standard Row and Column Algorithms

Algorithm 4 Standard column algorithm

```

1: for  $j : 2$  to  $N$  do
2:    $i \leftarrow 1$ 
3:   while  $i < j$  do
4:     if  $\text{low}(j) = \text{pivot}(i)$  then
5:        $\text{column } j \leftarrow \text{column } j \oplus \text{column } i$ 
6:       if  $\text{column } j$  is empty then
7:          $\text{low}(j) \leftarrow -1$  ▷ this column is reduced to  $\mathbf{0}$ 
8:         break
9:       else
10:         $i \leftarrow 1$ 
11:      else
12:         $i \leftarrow i + 1$ 
13:       $\text{pivot}(j) \leftarrow \text{low}(j)$ 

```

Algorithm 5 Standard row algorithm

```

1: for  $i : N$  to  $1$  do
2:   for  $j : 1$  to  $N$  do
3:     if  $\text{low}(j) = i$  then break
4:   if  $j = N + 1$  then continue
5:    $\text{pivot}(j) = \text{low}(j)$ 
6:   for  $k = j + 1$  to  $N$  do
7:     if  $\text{low}(k) = i$  then
8:        $\text{column } k \leftarrow \text{column } k \oplus \text{column } j$ 
9:       if  $\text{column } k$  is empty then
10:         $\text{low}(k) \leftarrow -1$  ▷ this column is reduced to  $\mathbf{0}$ 
11:         $\text{pivot}(k) \leftarrow -1$ 

```

B Algorithms to Compute Cohomology for Edges

Algorithm 6 Case 1 for edges

```

1: Input:  $(e, i_a, i_b, \delta_e)$ 
2: Output:  $(e, i_a, i_b, \delta_e)$ 
3:  $\{a, b\} \leftarrow f_1^{-1}(e)$ 
4: while  $i_a < N(a)$  AND  $i_b < N(b)$  do
5:   if  $f_0(n_{i_a}^a) < f_0(n_{i_b}^b)$  then
6:      $i_a \leftarrow i_a + 1$ 
7:   else if  $f_0(n_{i_a}^a) > f_0(n_{i_b}^b)$  then
8:      $i_b \leftarrow i_b + 1$ 
9:   else
10:    return  $(e, i_a, i_b, \langle f_1(\{a, b\}), n_{i_a}^a \rangle)$ 
11: return  $(e, i_a, i_b, \text{Empty})$ 

```

▷ Move to case 2

Algorithm 7 Case 2 for edges

```

1: Input:  $(e, i_a, i_b, \delta_e)$ 
2: Output:  $(e, i_a, i_b, \delta_e)$ 
3:  $\{a, b\} \leftarrow f_1^{-1}(e)$ 
4: while  $i_a < N(a)$  AND  $i_b < N(b)$  do
5:   if  $f_1(e_{i_a}^a) < f_1(e_{i_b}^b)$  then
6:      $\{a, d\} \leftarrow f_1^{-1}(e_{i_a}^a)$ 
7:     if  $d \in N^b$  AND  $f_1(\{b, d\}) < f_1(e_{i_a}^a)$  then
8:       return  $(e, i_a, i_b, \langle f_1(e_{i_a}^a), d \rangle)$ 
9:     else
10:       $i_a \leftarrow i_a + 1$ 
11:   else
12:      $\{b, d\} \leftarrow f_1^{-1}(e_{i_b}^b)$ 
13:     if  $d \in N^a$  AND  $f_1(\{a, d\}) < f_1(e_{i_b}^b)$  then
14:       return  $(e, i_a, i_b, \langle f_1(e_{i_b}^b), d \rangle)$ 
15:     else
16:       $i_b \leftarrow i_b + 1$ 
17:   while  $i_a < N(a)$  do
18:      $\{a, d\} \leftarrow f_1^{-1}(e_{i_a}^a)$ 
19:     if  $d \in N^b$  AND  $f_1(\{b, d\}) < f_1(e_{i_a}^a)$  then
20:       return  $(e, i_a, i_b, \langle f_1(e_{i_a}^a), d \rangle)$ 
21:     else
22:       $i_a \leftarrow i_a + 1$ 
23:   while  $i_b < N(b)$  do
24:      $\{b, d\} \leftarrow f_1^{-1}(e_{i_b}^b)$ 
25:     if  $d \in N^a$  AND  $f_1(\{a, d\}) < f_1(e_{i_b}^b)$  then
26:       return  $(e, i_a, i_b, \langle f_1(e_{i_b}^b), d \rangle)$ 
27:     else
28:       $i_b \leftarrow i_b + 1$ 
29: return  $(e, i_a, i_b, \text{Empty})$ 

```

Algorithm 8 FindSmallestt

```

1: Input:  $e$ 
2: Output:  $(e, i_a, i_b, \delta_e)$ 
3:  $\{a, b\} \leftarrow f_1^{-1}(e)$ 
4:  $i_a \leftarrow 0$ 
5:  $i_b \leftarrow 0$ 
6:  $\delta_0^e \leftarrow \text{Empty}$ 
7:  $(e, i_a, i_b, \delta_e) \leftarrow \text{Function Case1}((e, i_a, i_b, \delta_e))$ 
8: if  $low$  is Empty then
9:    $i_a \leftarrow$  smallest index s.t.  $f_1(e_{i_a}^a) > f_1(e)$ 
10:   $i_b \leftarrow$  smallest index s.t.  $f_1(e_{i_b}^b) > f_1(e)$ 
11:   $(e, i_a, i_b, \delta_e) \leftarrow \text{Function Case2}((e, i_a, i_b, \delta_e))$ 
12: return  $(e, i_a, i_b, \delta_e)$ 

```

Algorithm 9 FindNextt

```

1: Input:  $(e, i_a, i_b, \delta_e)$ 
2: Output:  $(e, i_a, i_b, \delta_e)$ 
3:  $\{a, b\} \leftarrow f_1^{-1}(e)$ 
4:  $\langle k^p, k^s \rangle \leftarrow \delta_i^e$ 
5: if  $k^p = f_1(e)$  then
6:   Increment  $i_a, i_b$  by 1
7:    $(e, i_a, i_b, \delta_{i+1}^e) \leftarrow \text{Function Case1}((e, i_a, i_b, \delta_i^e))$ 
8:   if  $\delta_{i+1}^e$  is Empty then
9:      $i_a \leftarrow$  smallest index s.t.  $f_1(e_{i_a}^a) > f_1(e)$ 
10:     $i_b \leftarrow$  smallest index s.t.  $f_1(e_{i_b}^b) > f_1(e)$ 
11:   else
12:     return  $(e, i_a, i_b, \delta_e)$ 
13: else
14:    $f_1(e_{i_a}^a) < f_1(e_{i_b}^b)$  ? increment  $i_a$  : increment  $i_b$ 
15:    $(e, i_a, i_b, \delta_e) \leftarrow \text{Function Case2}((e, i_a, i_b, \delta_e))$ 
16: return  $(e, i_a, i_b, \delta_e)$ 

```

C Algorithms to Compute Coboundary of Triangles

Algorithm 10 FindGEQt

```

1: Input:  $e, \delta_{\#}$ 
2: Output:  $(e, i_a, i_b, \delta_e)$ 
3:  $\{a, b\} \leftarrow f_1^{-1}(e)$ 
4:  $\langle k^p, k^s \rangle \leftarrow \delta_{\#}$ 
5: if  $k^p < f_1(e)$  then
6:    $(e, i_a, i_b, \delta_e) \leftarrow \text{Function FindSmallestt}(e)$ 
7:   return  $(e, i_a, i_b, \delta_e)$ 
8: else if  $k^p = f_1(e)$  then
9:    $i_a \leftarrow$  smallest index s.t.  $f_0(n_{i_a}^a) \geq k^s$ 
10:   $i_b \leftarrow$  smallest index s.t.  $f_0(n_{i_b}^b) \geq k^s$ 
11:  if  $f_0(n_{i_a}^a) = f_0(n_{i_b}^b)$  then
12:    return  $(e, i_a, i_b, \langle k^p, f_0(n_{i_a}^a) \rangle)$ 
13:  else
14:     $(e, i_a, i_b, \delta_e) \leftarrow \text{Function FindNextt}((e, i_a, i_b, \text{Empty}))$ 
15:    if  $\delta_e$  is not Empty then
16:      return  $(e, i_a, i_b, \delta_e)$ 
17:   $i_a \leftarrow$  smallest index s.t.  $f_1(e_{i_a}^a) \geq k^p$ 
18:   $i_b \leftarrow$  smallest index s.t.  $f_1(e_{i_b}^b) \geq k^p$ 
19:  if  $\langle k^p, k^s \rangle$  is in  $\delta_e$  then
20:    return  $(e, i_a, i_b, \langle k^p, k^s \rangle)$ 
21:   $(e, i_a, i_b, \delta_e) \leftarrow \text{Function Case2}((e, i_a, i_b, \delta_e))$ 
22:  return  $(e, i_a, i_b, \delta_e)$ 

```

Algorithm 11 Case1 for triangles

```

1: Input:  $(t, i_a, i_b, i_c, f, \delta_t)$ 
2: Output: 1 or 0
3:  $\langle k^p, k^s \rangle \leftarrow f_2(t)$ 
4:  $a \leftarrow \min\{f_1^{-1}(k^p)\}$ 
5:  $b \leftarrow \max\{f_1^{-1}(k^p)\}$ 
6:  $c \leftarrow k^s$ 
7: while  $i_c < N(a)$  AND  $f_1(e_{i_c}^c) < k^p$  do
8:    $\{c, d\} \leftarrow e_{i_c}^c$ 
9:   if  $f_1(\{a, d\})$  and  $f_1(\{b, d\})$  are less than  $k^p$  then
10:     $f \leftarrow 0$ 
11:     $\delta_t \leftarrow \langle k^p, f_1(e_{i_c}^c) \rangle$ 
12:    return 1
13:    $i_c \leftarrow i_c + 1$ 
14: return 0

```

Algorithm 12 Case 2 for triangles

```

1: Input:  $(t, i_a, i_b, i_c, f, \delta_t)$ 
2:  $\langle k^p, k^s \rangle \leftarrow f_2(t)$ 
3:  $a \leftarrow \min\{f_1^{-1}(k^p)\}$ 
4:  $b \leftarrow \max\{f_1^{-1}(k^p)\}$ 
5:  $c \leftarrow k^s$ 
6: while not reached end of all  $E^a, E^b, E^c$  do
7:    $o_* \leftarrow \min\{f_1(e_{i_a}^a), f_1(e_{i_b}^b), f_1(e_{i_c}^c)\}$  ▷ Exclude indices that reach end of edge-nbd
8:    $\{v_1, d\} \leftarrow f_1^{-1}(o_*)$ 
9:    $\{v_2, v_3\} \leftarrow \{a, b, c\} \setminus \{v_1\}$ 
10:  if  $f_1(\{v_2, d\})$  and  $f_1(\{v_3, d\})$  are less than  $o_*$  then
11:     $\delta_t \leftarrow \langle o_*, f_1(\{v_2, v_3\}) \rangle$ 
12:     $f \leftarrow 1$  if  $v_1 = a$ ;  $2$  if  $v_1 = b$ ;  $3$  if  $v_1 = c$ 
13:    return
14:  else
15:    Increment  $i_{v_1}$ 
16:  $\delta_t \leftarrow \text{Empty}$ 
17:  $f \leftarrow -1$ 

```

Algorithm 13 FindSmallesth

```

1: Input:  $(t, i_a, i_b, i_c, f, \delta_t)$ 
2:  $i_c \leftarrow 0$ 
3: if Function Case1 $(t, i_a, i_b, i_c, f, \delta_t)$  then
4:   return
5:  $\langle k^p, k^s \rangle \leftarrow t$ 
6:  $\{a, b\} \leftarrow f_1^{-1}(k^p)$ 
7:  $i_a \leftarrow \underset{i_a}{\operatorname{argmin}}(f_1(e_{i_a}^a) \geq k^p)$ 
8:  $i_b \leftarrow \underset{i_b}{\operatorname{argmin}}(f_1(e_{i_b}^b) \geq k^p)$ 
9: Increment  $i_a, i_b$ 
10: Function Case2 $(t, i_a, i_b, i_c, f, \delta_t)$ 

```

Algorithm 14 FindNexth for triangles

```

1: Input:  $(t, i_a, i_b, i_c, f, \delta_t)$ 
2:  $\langle k^p, c \rangle \leftarrow f_2(t)$ 
3:  $a \leftarrow \min\{f_1^{-1}(k^p)\}$ 
4:  $b \leftarrow \max\{f_1^{-1}(k^p)\}$ 
5:  $c \leftarrow k^s$ 
6: if  $f = 0$  then
7:   Increment  $i_c$ 
8:   if Function Case1 $(t, i_a, i_b, i_c, f, \delta_t)$  then
9:     return
10:   $i_a \leftarrow \underset{i_a}{\operatorname{argmin}}(f_1(e_{i_a}^a) \geq k^p)$ 
11:   $i_b \leftarrow \underset{i_b}{\operatorname{argmin}}(f_1(e_{i_b}^b) \geq k^p)$ 
12:  Increment  $i_a, i_b$ 
13: if Not moving from Case1 then
14:   if  $f = 1$  then
15:      $i_a \leftarrow i_a + 1$ 
16:   else if  $f = 2$  then
17:      $i_b \leftarrow i_b + 1$ 
18:   else if  $f = 3$  then
19:      $i_c \leftarrow i_c + 1$ 
20: Function Case2 $(t, i_a, i_b, i_c, f, \delta_t)$ 

```

Algorithm 15 FindGEQh for triangles

```

1: Input:  $(t, i_a, i_b, i_c, f, \delta_t), \delta_{\#}$ 
2:  $\langle k_{\#}^p, k_{\#}^s \rangle \leftarrow \delta_{\#}$ 
3:  $\langle k^p, c \rangle \leftarrow t$ 
4:  $\{a, b\} \leftarrow f_1^{-1}(k^p)$ 
5: if  $k_{\#}^p < k^p$  then
6:   Function FindSmallesth( $t, i_a, i_b, i_c, f, \delta_t$ )
7:   return
8: else if  $k_{\#}^p = k^p$  then
9:    $i_c \leftarrow \underset{i_c}{\operatorname{argmin}}(f_1(e_{i_c}^c) \geq k_{\#}^s)$ 
10:  if  $f_1(e_{i_c}^c) = k_{\#}^s$  then
11:     $\delta_t \leftarrow \delta_{\#}$ 
12:     $v \leftarrow 0$ 
13:    return
14:  if Function Case1( $t, i_a, i_b, i_c, f, \delta_t$ ) then
15:    return
16:   $i_a \leftarrow \underset{i_a}{\operatorname{argmin}}(f_1(e_{i_a}^a) \geq k^p)$ 
17:   $i_b \leftarrow \underset{i_b}{\operatorname{argmin}}(f_1(e_{i_b}^b) \geq k^p)$ 
18:  Increment  $i_a, i_b$ 
19: else
20:   $i_a \leftarrow \underset{i_a}{\operatorname{argmin}}(f_1(e_{i_a}^a) \geq k_o^p)$ 
21:   $i_b \leftarrow \underset{i_b}{\operatorname{argmin}}(f_1(e_{i_b}^b) \geq k_o^p)$ 
22:   $i_c \leftarrow \underset{i_c}{\operatorname{argmin}}(f_1(e_{i_c}^c) \geq k_o^p)$ 
23: while 1 do
24:  Function Case2( $t, i_a, i_b, i_c, f, \delta_t$ )
25:  if  $\delta_t \geq \delta_{\#}$  OR  $\delta_t$  is Empty then
26:    break
27:  if  $f = 1$  then
28:     $i_a \leftarrow i_a + 1$ 
29:  else if  $f = 2$  then
30:     $i_b \leftarrow i_b + 1$ 
31:  else if  $f = 3$  then
32:     $i_c \leftarrow i_c + 1$ 

```

D Algorithms for Serial-parallel Cohomology Reduction of Triangles

Algorithm 16 SerialParallel: Reduction of triangles

```

1: Function SerialParallelReduce
2:   Function ParallelReduce
3:   Function SerialReduce
4:   Function Clearance
5: EndFunction

6: Input  $F_1$ , batch-size
7:  $V^\perp, \mathbf{v} \leftarrow []$ 
8:  $i \leftarrow 0$ 
9: for  $e$  in  $F_1^{-1}$  do
10:  Compute  $\delta e$  and sort it along  $F_2^{-1}$ 
11:  for  $t$  in  $\delta e$  with  $d(t) = e$  do
12:     $(t, i_a, i_b, i_c, f, \delta_t) \leftarrow$  Function FindSmallesth( $t$ )
13:    if  $\delta_1^t$  is Empty then
14:      continue
15:     $v_i \leftarrow [(t, i_a, i_b, i_c, f, \delta_t)]$ 
16:     $\delta_*^{v_i} \leftarrow \delta_t$ 
17:     $f_e \leftarrow 0$ 
18:    Append  $(t, v_i, \delta_*^{v_i}, f_v, f_r, f_a, f_e)$  to  $\mathbf{v}$ 
19:     $i \leftarrow i + 1$ 
20:    if  $i =$  batch-size then
21:      Function SerialParallelReduce

22: while  $i > 0$  do
23:   Function SerialParallelReduce

```

Algorithm 17 Parallel reduction

```

1: Input:  $\mathbf{v}, V^\perp, p^\perp$ 
2: Output:  $\mathbf{v}$ 
3: for  $(t, v_i, \delta_*^{v_i}, f_v, f_r, f_a, f_e)$  in  $\mathbf{v}$  do ▷ Embarrassingly parallel
4:    $f_r \leftarrow 0$ 
5:    $f_a \leftarrow 1$ 
6:   if  $(\delta_*^{v_i}, t)$  is a trivial persistence pair then
7:     continue
8:   while  $(\delta_*^{v_i}, t')$  is a trivial persistence pair OR is in  $p^\perp$  do
9:      $(t', i_a, i_b, i_c, v, \delta_{t'}) \leftarrow$  Function FindGEQt( $t', \delta_*^{v_i}$ )
10:    Append  $(t', i_a, i_b, i_c, f, \delta_{t'})$  to  $v_i$ 
11:    for  $t_k$  in  $V^\perp(t')$  do
12:       $(t_k, i_a, i_b, i_c, f, \delta_{t_k}) \leftarrow$  Function FindGEQt( $t_k, \delta_*^{v_i}$ )
13:      Append  $[(t_k, i_a, i_b, i_c, f, \delta_{t_k})]$  to  $v_i$ 
14:      Implicit column algorithm to update  $\delta_*^{v_i}$ 
15:      if  $\delta_*^{v_i}$  is Empty then
16:         $f_e \leftarrow 1$ 
17:      return

```

Algorithm 18 Serial reduction

```

1: for  $(t, v_i, \delta_*^{v_i}, f_r^i, f_v^i, f_a^i, f_e^i)$  in  $\mathbf{v}$  do
2:   if  $f_e^i$  OR  $f_v^i$  then
3:     continue
4:    $j \leftarrow 1$ 
5:   while  $j < i$  do
6:     if  $f_e^j$  then
7:        $j \leftarrow j + 1$ 
8:     continue
9:     if  $\delta_*^{v_j} > \delta_*^{v_i}$  then
10:       $j \leftarrow j + 1$ 
11:     continue
12:     if  $\delta_*^{v_j} < \delta_*^{v_i}$  then
13:       if  $f_r^j$  OR  $f_v^j$  then
14:          $f_a^i \leftarrow 0$ 
15:         break
16:        $j \leftarrow j + 1$ 
17:     continue
18:     Append  $v_j$  to  $v_i$ 
19:     Fast implicit column algorithm to update  $\delta_*^{v_i}$ 
20:     if  $\delta_*^{v_i}$  is Empty then
21:        $f_e^i \leftarrow 1$ 
22:       break
23:     if  $\exists t'$  s.t.  $(\delta_*^{v_i}, t')$  is a trivial pair then
24:        $f_v^i \leftarrow 1$ 
25:        $f_r^i \leftarrow 0$ 
26:        $f_a^i \leftarrow 0$ 
27:       break
28:     if  $(\delta_*^{v_i}, t')$  is a persistence pair in  $p^\perp$  then
29:        $f_v^i \leftarrow 0$ 
30:        $f_r^i \leftarrow 1$ 
31:        $f_a^i \leftarrow 0$ 
32:       break
33:    $j \leftarrow 1$ 

```

Algorithm 19 Clearance

```

1: for  $(t, v_i, \delta_*^{v_i}, f_v, f_r, f_a, f_e)$  in  $\mathbf{v}$  do
2:   if  $f_e = 0$  then
3:     Non-contractible cycle born at  $t$ 
4:     Remove  $(t, v_i, \delta_*^{v_i}, f_v, f_r, f_a, f_e)$  from  $\mathbf{v}$ 
5:     continue
6:   if  $f_a = 1$  then
7:     Store  $(\delta_*^{v_i}, t)$  in  $p^\perp(t)$ 
8:     Define  $T \leftarrow [t_k \text{ in } v_i = [(t_k, i_a, i_b, i_c, f, \delta_*^{t_k})]]$  with  $t_k \neq t$ 
9:     Remove triangles from  $T$  that occur even number of times (modulo 2 sum)
10:     $V^\perp(t) \leftarrow T$ 
11:    Remove  $(t, v_i, \delta_*^{v_i}, f_v, f_r, f_a, f_e)$  from  $\mathbf{v}$ 

```

Data set	Fast Imp. col.	Imp. row
dragon	(2.859 s, 262 MB)	(2.887 s, 270 MB)
fractal	(32.1 s, 695 MB)	(29.848 s, 670 MB)
o3	(4.989 s, 157 MB)	(22.7 s, 140 MB)
torus4(1)	(9.4 s, 328 MB)	(44.47 s, 295 MB)
torus4(2)	(41.2 s, 1 GB)	(74.6 s, 1 GB)
Hi-C (control)	(263 s, 6.23 GB)	(595 s, 7.19 GB)
Hi-C (Auxin) (102 s, 3.98 GB)	(123 s, 3.83 GB)	

Table 4: Comparing fast implicit column algorithm (Dory compiled with `-D SAVEPD`) and implicit row algorithm (both serial-parallel over 4 threads). Time taken (seconds) was measured using the command `time` in terminal of macOS. Peak memory usage is recorded using application Instruments in macOS.

Data set	n	τ_m	d	Gudhi	Eirene
dragon	2000	∞	1	NA	7.4 GB
fractal	512	∞	2	NA	9.13 GB
o3	8192	1	2	2.3 GB	9.34 GB
torus4(1)	50000	0.15	1	3 GB	126 GB
torus4(2)	50000	0.15	2	30 GB	NA

Table 5: Benchmarks for Gudhi and Eirene. NA means that the data set was not processed within 10 mins. or the system ran out of memory.

E Computation and Benchmarks

Base memory used by Dory

F_1 : (two vertices per edge) + (pointer to every edge) + (length of every edge) = $2n_e + n_e + n_e = 4n_e$.

Lengths of neighborhoods: one for every vertex = n .

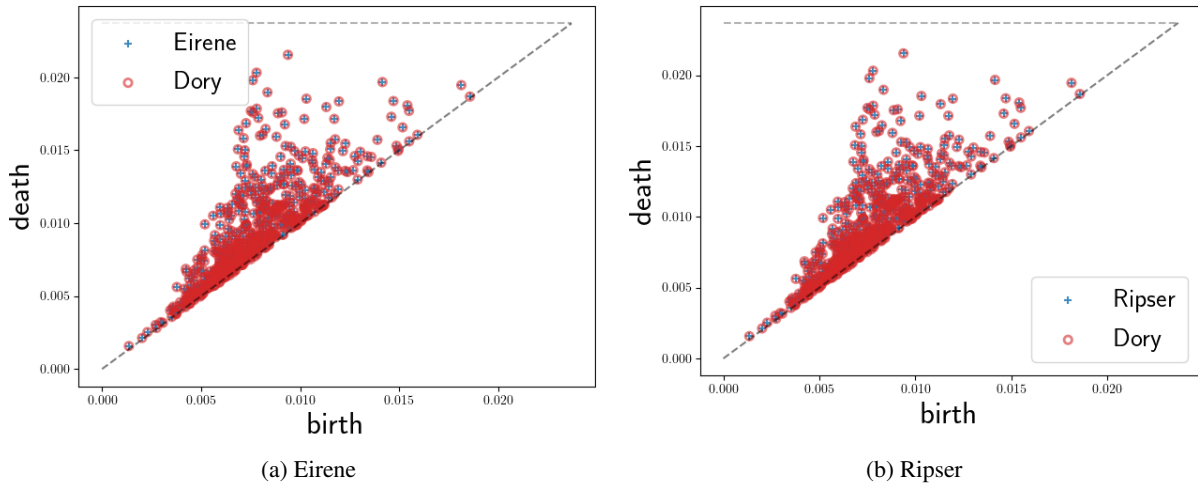
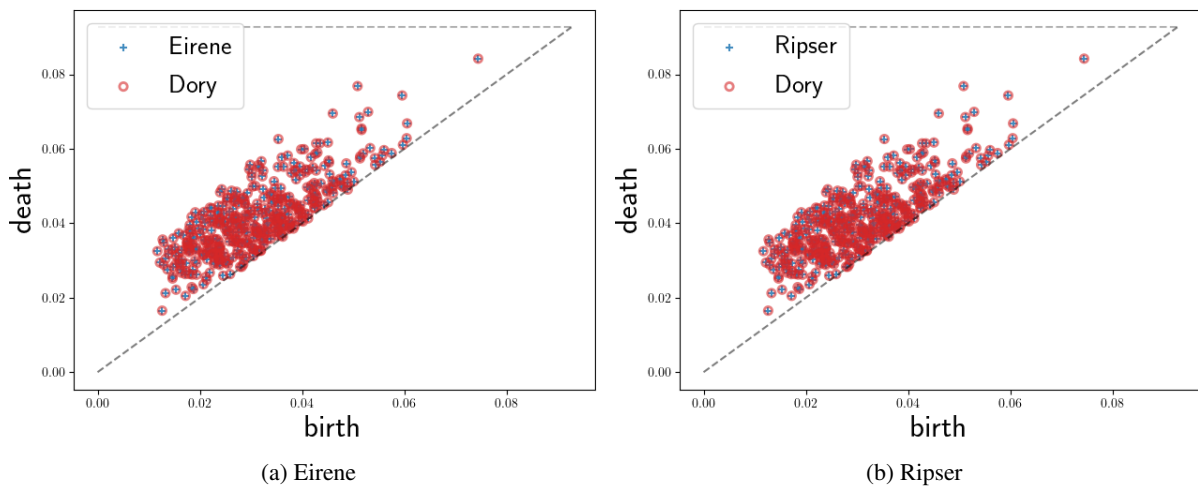
Vertex-neighborhood:(every edge is in two neighborhoods)*(neighbor and order are stored) + (pointer for every vertex) = $(2n_e) * 2 + n = 4n_e + n$.

Edge-neighborhood = Vertex-Neighborhood = $4n_e + n$.

Fast implicit col and implicit row algorithm

Gudhi and Eirene

The peak memory usage by Gudhi (v. 3.4.0) was recorded using the package `memory-profiler` (v. 0.57.0) in Python (v. 3.8.5), and the memory used by Eirene (v. 1.3.5) was estimated by observing `activity monitor` of macOS because the memory profiling tools in Julia (v. 1.5) report cumulative memory allocations instead of the net memory in use.

F Persistence Diagrams for Data SetsFigure 22: Dragon H_1 PDFigure 23: Fractal H_1 PD

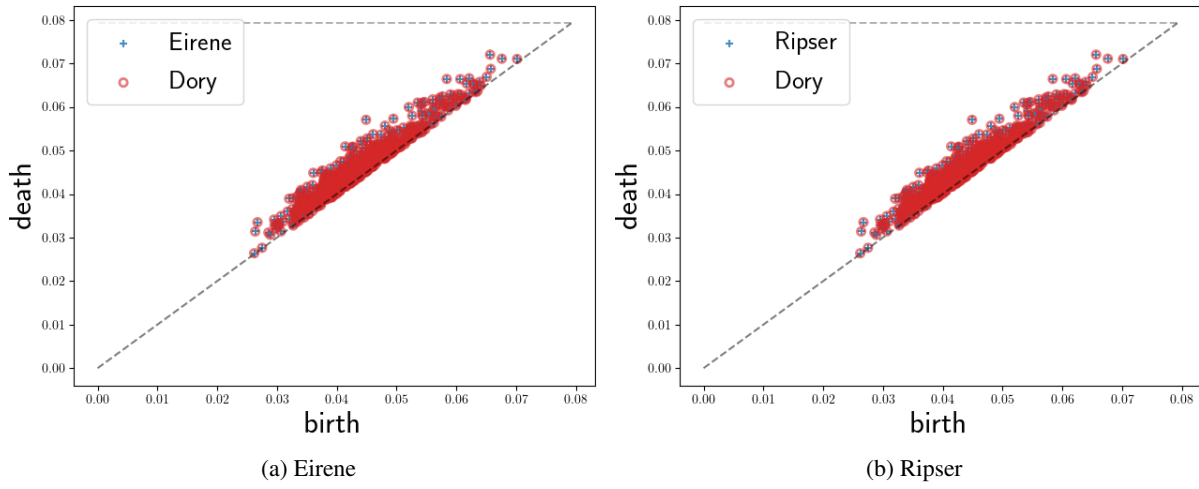


Figure 24: Fractal H_2 PD

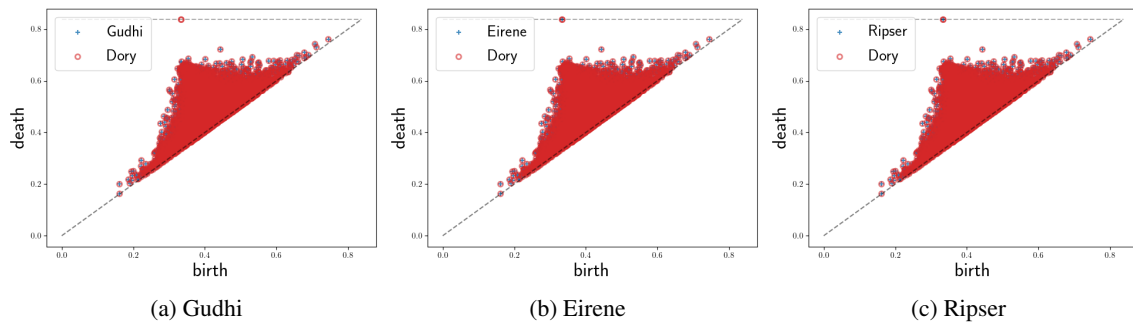


Figure 25: $o_3 H_1$ PD

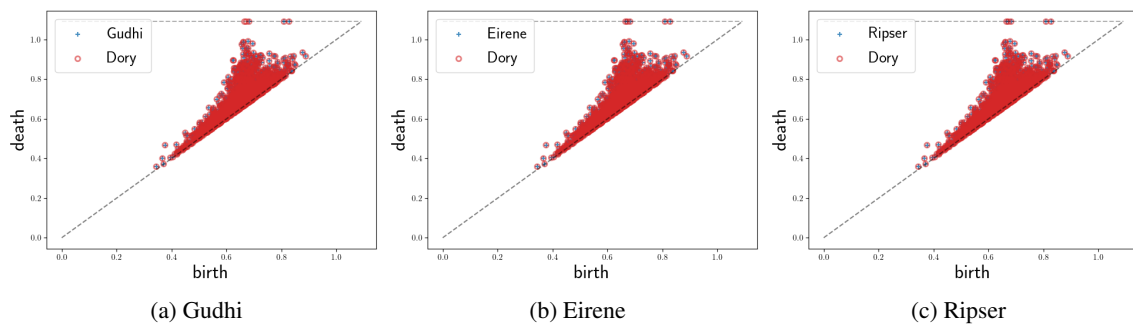


Figure 26: $o_3 H_2$ PD

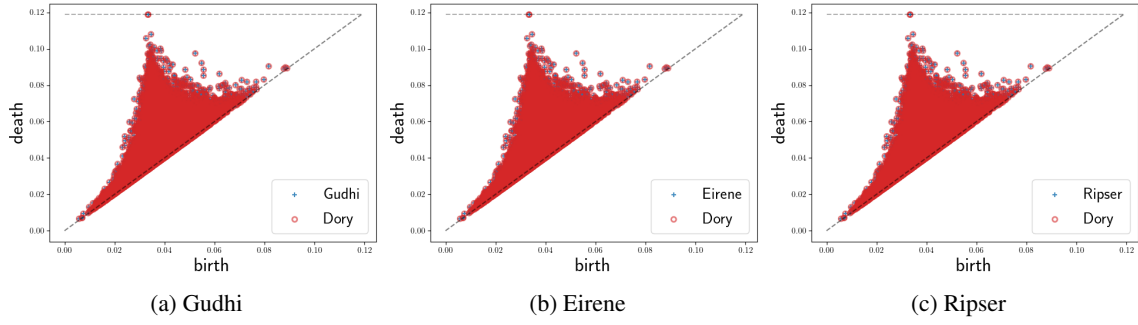


Figure 27: torus H_2 PD

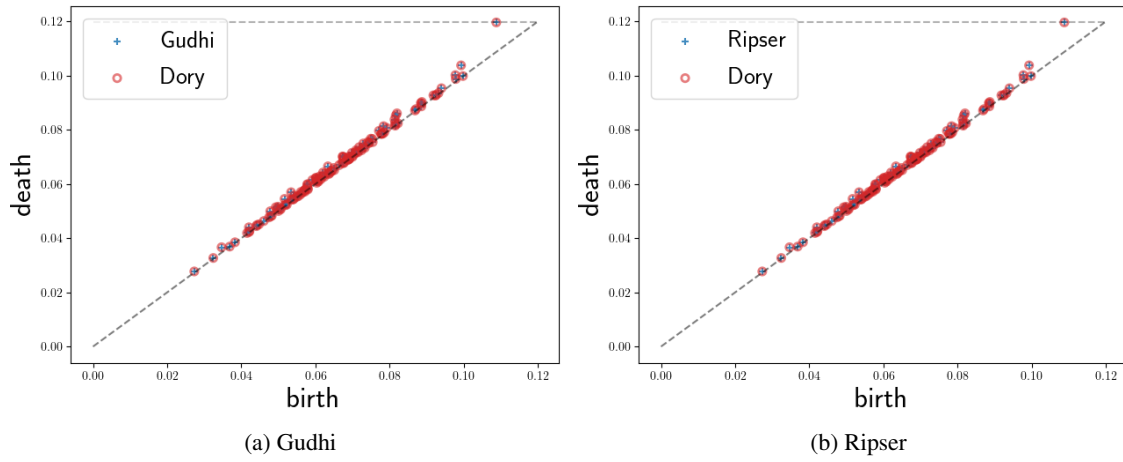
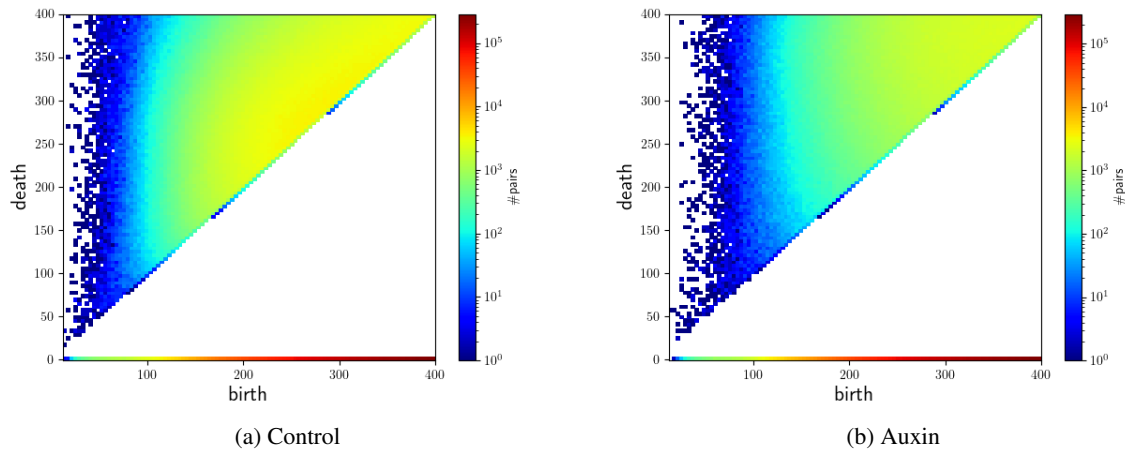
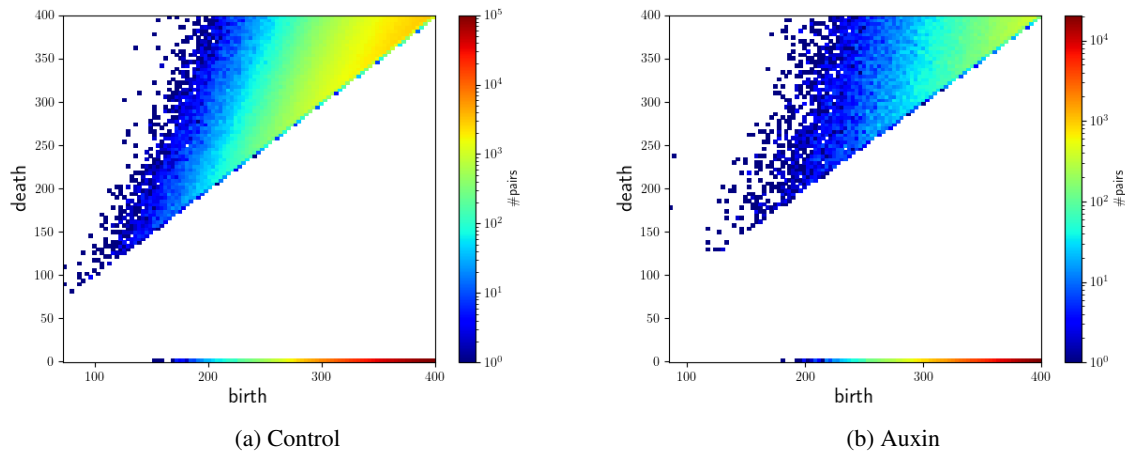


Figure 28: torus H_2 PD

G Persistence Diagrams for Hi-C

Figure 29: Hi-C data sets H_1 PDFigure 30: Hi-C data sets H_2 PD

References

- Herbert Edelsbrunner and John Harer. Persistent homology—a survey. *Contemporary mathematics*, 453:257–282, 2008.
- Vin De Silva, Dmitriy Morozov, and Mikael Vejdemo-Johansson. Dualities in persistent (co) homology. *Inverse Problems*, 27(12):124003, 2011.
- Jean-Daniel Boissonnat and Clément Maria. The simplex tree: an efficient data structure for general simplicial complexes. *Algorithmica*, 70(3):406–427, 2014.
- Ulrich Bauer. Ripser: efficient computation of vietoris-rips persistence barcodes. *arXiv preprint arXiv:1908.02518*, 2019.
- M Jordan Rowley and Victor G Corces. Organizational principles of 3d genome architecture. *Nature Reviews Genetics*, 19(12):789–800, 2018.
- Erez Lieberman-Aiden, Nynke L Van Berkum, Louise Williams, Maxim Imakaev, Tobias Ragozy, Agnes Telling, Ido Amit, Bryan R Lajoie, Peter J Sabo, Michael O Dorschner, et al. Comprehensive mapping of long-range interactions reveals folding principles of the human genome. *science*, 326(5950):289–293, 2009.
- Suhas SP Rao, Miriam H Huntley, Neva C Durand, Elena K Stamenova, Ivan D Bochkov, James T Robinson, Adrian L Sanborn, Ido Machol, Arina D Omer, Eric S Lander, et al. A 3d map of the human genome at kilobase resolution reveals principles of chromatin looping. *Cell*, 159(7):1665–1680, 2014.

- Suhas SP Rao, Su-Chen Huang, Brian Glenn St Hilaire, Jesse M Engreitz, Elizabeth M Perez, Kyong-Rim Kieffer-Kwon, Adrian L Sanborn, Sarah E Johnstone, Gavin D Bascom, Ivan D Bochkov, et al. Cohesin loss eliminates all loop domains. *Cell*, 171(2):305–320, 2017.
- Herbert Edelsbrunner, David Letscher, and Afra Zomorodian. Topological persistence and simplification. In *Proceedings 41st annual symposium on foundations of computer science*, pages 454–463. IEEE, 2000.
- David Cohen-Steiner, Herbert Edelsbrunner, and Dmitriy Morozov. Vines and vineyards by updating persistence in linear time. In *Proceedings of the twenty-second annual symposium on Computational geometry*, pages 119–126, 2006.
- Chao Chen and Michael Kerber. Persistent homology computation with a twist. In *Proceedings 27th European Workshop on Computational Geometry*, volume 11, pages 197–200, 2011.
- Nina Otter, Mason A Porter, Ulrike Tillmann, Peter Grindrod, and Heather A Harrington. A roadmap for the computation of persistent homology. *EPJ Data Science*, 6(1):17, 2017.
- Jesse R Dixon, Siddarth Selvaraj, Feng Yue, Audrey Kim, Yan Li, Yin Shen, Ming Hu, Jun S Liu, and Bing Ren. Topological domains in mammalian genomes identified by analysis of chromatin interactions. *Nature*, 485(7398): 376–380, 2012.
- Tamal K Dey, Dayu Shi, and Yusu Wang. Simba: An efficient tool for approximating rips-filtration persistence via simplicial batch collapse. *Journal of Experimental Algorithmics (JEA)*, 24:1–16, 2019.
- Anirudh Som, Hongjun Choi, Karthikeyan Natesan Ramamurthy, Matthew P Buman, and Pavan Turaga. Pi-net: A deep learning approach to extract topological persistence images. In *Proceedings of the IEEE/CVF Conference on Computer Vision and Pattern Recognition Workshops*, pages 834–835, 2020.